Università Campus Bio-Medico di Roma

Corso di dottorato di ricerca in
Scienze e Ingegneria per l'Uomo e
l'Ambiente XXXVII ciclo
a.a. 2021-2022

Robotic-Assisted Transcranial Magnetic Stimulation: Development and Validation of Advanced Protocols for Precision Brain Stimulation

Annamaria Palese

Coordinatore
Prof. Giulio Iannello

Tutore
Prof. Giovanni Di Pino
Prof. Domenico Formica

Ottobre 2025

Abstract

Transcranial Magnetic Stimulation (TMS) is a non-invasive brain stimulation technique used to modulate cortical excitability by generating brief-lasting and high-intensity magnetic fields which bypass the skull and induce an electric field in the cerebral cortex. TMS has been widely employed in clinical settings to treat neurological conditions (e.g., migraine, tinnitus, neuropathic pain) and psychiatric disorders (e.g., major depressive disorder, obsessive–compulsive disorder, addiction), as well as in research to investigate brain functional organization, connectivity and neuronal plasticity. However, the conventional TMS administration is affected by coil placement inaccuracies, operator-dependent variability, and the lack of subject-specific protocol adaptation.
This issue is addressed in the present work by designing and validating a modular, high-performance, and economically sustainable robot-aided TMS platform able to deliver TMS simulation with minimal positional and orientation errors and with great versatility. The proposed system was assessed in both static conditions, replicating conventional experimental setups where the subject remains stationary, and dynamic conditions, allowing head rotations, translations, and more complex motion patterns similar to those occurring during walking. Implementing and assessing different control strategies, the results showed that hybrid force-position control performs better under dynamic conditions, while selective impedance is more suitable for static ones, suggesting the opportunity to develop a platform capable of dynamically switching between the two strategies according to operational requirements.

Successively, robot-aided TMS was then employed to develop and implement more advanced stimulation paradigms which would be exceedingly challenging for a human operator. A robot-aided rTMS protocol combined with a priming paradigm was proposed to explore whether direction-specific neuronal populations in the primary motor cortex (M1) can be selectively modulated during movement preparation, hilighting how the accuracy and rapidity offered by the robotic platform enable experimental designs that were previously difficult to achieve. Lastly, robot-aided TMS was combined with EEG to achieve precise spatial targeting and temporal alignment of stimulation. Through an EEG-informed TMS approach, stimulation was synchronized with specific phases of each participant's mu rhythm, revealing a phase-dependent modulation of corticospinal excitability and supporting the important role of cortical state in shaping stimulation effects.
In conclusion, this work, by introducing advanced engineering strategies into the field of TMS, demonstrates how methodological innovation can drive the development of more reliable, individualized, and effective stimulation protocols.

List of Publications

[1] Annamaria Palese*, Alessia Noccaro*, François Le Jeune et al. “Evaluation of control approaches for TMS robot-aided platform during head motion”. 2025, *In preparation.*

[2] Annamaria Palese*, Marianna Lanza*, et al. “Automated Transcranial Magnetic Stimulation (TMS) Platforms: Technological Advances and Clinical and Research Applications”. 2025, *In preparation.*

[3] Annamaria Palese, Francesca Fiori, et al. “Robot-Aided rTMS to Probe Directional Representations in Human Primary Motor Cortex (M1): A Pilot Study”. Poster and abstract presented at the *15th International Conference on Bioelectromagnetism (ICBEM 2024)*, Espoo, Finland.

[4] Annamaria Palese*, Mirja Osnabrugge*, et al. “Cortical Excitability Profile of the Sensory Motor Mu Rhythm”. 2025, *In preparation.*

Contents

List of Figures

List of Tables

Chapter 1

Introduction

The evolution of medicine has always mirrored technological progress and socio-economic transformations (Fig. 1.1). Today, it is moving into a new era: *Healthcare 5.0*, which combines the principles of *Industry 4.0* with a human-centred approach to deliver smart, adaptive and personalized medical services [1].
In the same direction, non-invasive brain stimulation techniques, in particular Transcranial Magnetic Stimulation (TMS), have also advanced rapidly toward customized and precise interventions.
In 1896, Arsène d'Arsonval explored the physiological effects of magnetic fields on the human brain and, almost a century later, in 1985, Anthony T. Barker introduced the first modern device for TMS [2], [3].
TMS operates according to Faraday's law of electromagnetic induction: a brief-lasting and high-intensity current crosses a coil placed tangentially on the scalp and generates a time-varying magnetic field that induces an electric field in the cerebral cortex [4].

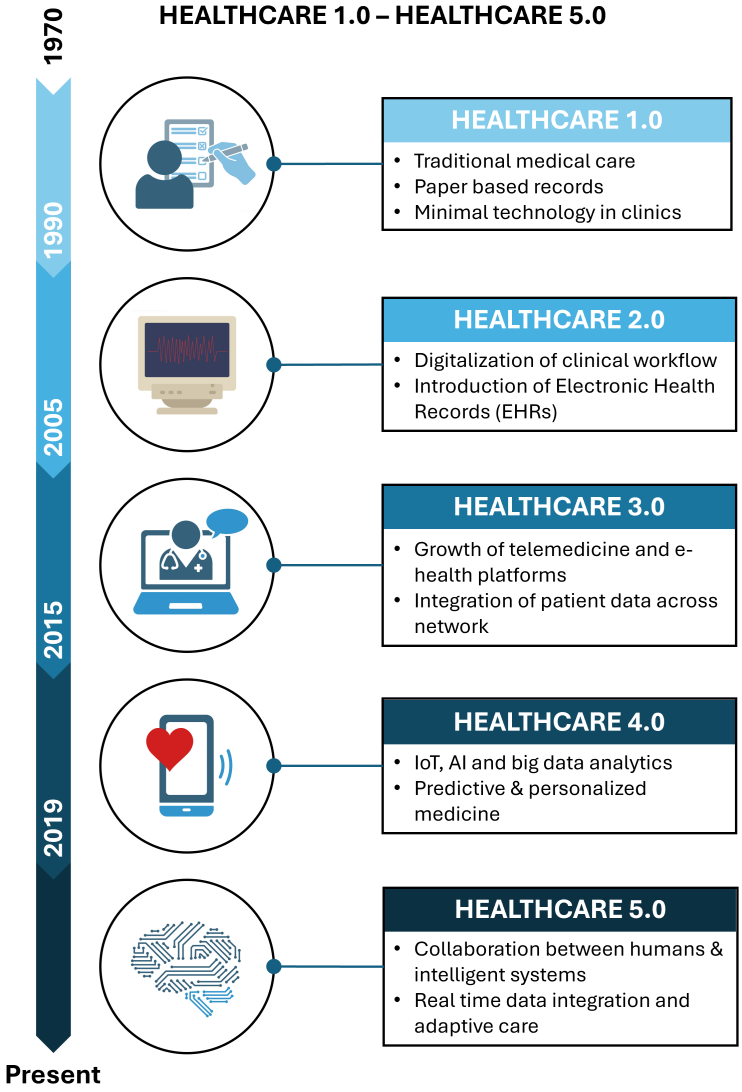

Fig. 1.1 The evolution of healthcare systems: from healthcare 1.0 to healthcare 5.0.

By modulating cortical excitability, TMS is employed to investigate functional brain organization and connectivity [5], but also to assess corticospinal integrity and to treat a wide variety of neurological conditions (e.g, migraine, tinnitus, neuropathic pain, Parkinson's disease and post-stroke rehabilitation) [6], and psychiatric disorders (e.g, major depressive disorder, obsessive–compulsive disorder, addiction) [7].

Although TMS has a highly safe profile and is widely used, its standard

administration suffers from limitations that compromise the accuracy and reproducibility of its outcomes. Several factors affect the effectiveness of stimulation, including spatial and operator-dependent variables. For instance, minor translations or rotations with respect to the optimal coil placement or variations in the distance between the scalp and coil may alter the intensity and the spatial direction of the cortical induced electric field (E-field) and stimulate adjacent areas instead of the target region [8], [9].
Furthermore, current clinical practice in TMS often follows a one-size-fits-all approach. Treatments are administered according to standardized protocols which do not consider inter-individual variability in anatomical structure, functional organization, or neurophysiological dynamics [10], [11].
Due to this lack of personalization, TMS clinical efficacy remains highly variable, and many patients experience little to no meaningful improvement. In this scenario, the need for a transformation in the TMS field arises and finds its most promising answer in the integration of high-precision robotic automation with personalized neuromodulation methods.
Accordingly to the Healthcare 5.0 paradigm, this transition is not only about technological progress, but also a complete conceptual redefinition of therapeutic practice: from a standardized procedure to an intelligent, adaptive, and patient-centered intervention.

1.1 Thesis Outline

In this emerging technological and clinical landscape, the contribution of this thesis is a structured investigation into the core components of next-generation brain stimulation. To guide the reader through its contents, the structure of the thesis is outlined below.

Chapter 2,*"Automated transcranial magnetic stimulation (TMS) platforms: Technological Advances and Clinical and Research Applications"*,

provides a systematic overview of the current state of the automation in TMS. The evolution of TMS platforms from manual to automated configurations is examinated, with a particular focus on their technological architectures and on the potential and current implications for clinical and research routine care. This chapter outlines the theoretical background and rationale behind the technological developments presented in subsequent chapters.

Chapter 3,*"From Technological Designing to Neuroscientific Application: Experimental Studies with a Robot-Aided TMS Platform"*, opens with a brief introduction in the **Section 3.1** outlining the *fil rouge* that connects the three studies forming the core of this thesis. Subsequently, the **Section 3.2** focuses on the first study: *"Optimized Robot-Aided Transcranial Magnetic Stimulation (TMS) Platform: Evaluation of Control Approaches for Head Motion Compensation"*, which proposes and assesses a robot-aided TMS platform developed to deliver stimulation with high accuracy even in the presence of patient head movements. A comparative evaluation of four control strategies for coil placement is conducted to assess their positioning and orientation accuracy and their contact force in both static and dynamic conditions. This work opens the gates towards the implementation of new TMS protocols during the execution of complex motor tasks, fully exploiting the potential of robotic technologies. This perspective could allow us to have a deeper insight of how the brain organizes complex movements and adapts to motor learning, and to identify more targeted and effective rehabilitation strategies for patients with movement disorders.
The following **Section 3.3**, *"Robot-Aided Repetitive TMS (rTMS) to Probe Directional Representations in Human Primary Motor Cortex (M1): A Pilot Study"*, describes the second study. It presents a pilot implementation of a robot-aided rTMS paradigm designed to test whether direction-specific neuronal populations in primary motor cortex (M1) can be selectively modulated during movement preparation. The study highlights the methodological challenges that future research must address to advance toward precision TMS

protocols.
Finally, the **Section 3.4**, proposes the last and third study: *Robot-Aided EEG-Informed TMS: Phase-Specific Modulation of the Mu Rhythm*, which addresses the question of determining the optimal timing for stimulation delivery. A novel EEG-informed TMS method is presented: by aligning stimulation with specific phases of the mu rythm, the section presents an approach to improve the temporal precision of stimulation and offers new insights into how brain state-dependent stimulation can modulate corticospinal excitability.

Chapter 4, *Conclusion and Future Outlook*, summarizes the principal findings of this thesis, outlines its limitations, and suggests potential directions for future reserach.

Chapter 2

Automated Transcranial Magnetic Stimulation (TMS) Platforms: Technological Advances and Clinical and Research Applications

2.1 Background

Transcranial Magnetic Stimulation (TMS) is a non-invasive brain stimulation technique that uses strong time-varying magnetic fields which bypass the skull and induce cortical electric currents capable of modulating neuronal firing and changing cortical excitability (Fig. 2.1) [4]. Magnetic pulses are delivered through a coil placed tangentially to the scalp over the stimulation site, typically identified through craniometric landmarks (e.g., Beam F3, 5 cm rule) and refined with MRI-based neuronavigation [12], [13].

Since its introduction in 1985 [3], TMS has been widely used in clinical settings for diagnostics and follow-up of multiple sclerosis [15], [16], as well as in treating a range of neurological disorders such as stroke [17], [18], [19], chronic pain [20], migraine [21], [22], and amyotrophic lateral sclerosis [23], [24]. Moreover, in the last years, growing evidence has also shown significant

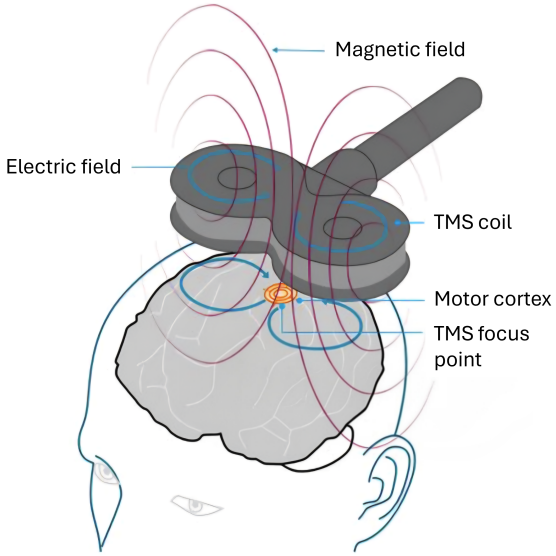

Fig. 2.1 Schematic representation of the physical principle underlying transcranial magnetic stimulation (TMS). A rapidly changing electric current flows through the TMS coil, generating a magnetic field that penetrates the scalp and skull. This time-varying magnetic field induces an electric current in the underlying cortical tissue, leading to neuronal activating. Adapted from [14].

TMS effects in alleviating symptoms related to psychiatric disorders such as depression [25], [26] and addiction [27], [28], [29].
However, TMS is not only employed in clinical treatments but also in research applications to investigate brain function, connectivity, and neural plasticity [26], [30].
Unlike purely observational methods, such as functional magnetic resonance imaging (fMRI), TMS transiently perturbs the cortical activity in targeted brain regions and provides a method to explore causal relationships between neural circuits and cognitive or behavioural processes [30], [31].
In standard TMS protocols, an experienced operator places the coil over the subject's head and holds it over the stimulation target for the entire session [32]. This activity is physically and cognitive demanding: the coil weight and the prolonged treatment duration require sustained operator effort [33].
Operator fatigue, over time, may affect coil positioning accuracy, and reduce

the treatment efficacy [34]. Indeed, even small variations from the optimal coil placement [35], [36], [37], [38] can alter the intensity and the direction of the induced electric field, and stimulate adjacent cortical areas instead of the target region [39], [40], [41]. In high-volume clinical settings, where multiple TMS treatment sessions are frequently administered in rapid succession, cumulative operator fatigue can gradually decrease positioning accuracy and, in turn, limit the number of treatments that can be daily performed.
Moreover, patients must remain still throughout the TMS procedure, as even slight involuntary head movements can cause coil misalignment [42].
To prevent this, the operator usually applies a manual pressure on the scalp through the coil for its stabilization and this might induce pain or discomfort and affect the patient's experience and the treatment tolerability [43].
In the early 2000s, robot-aided TMS platforms have started to be developed to overcome some of the limitations of manual TMS administration.
These platforms automatically places and maintain the coil stable at the stimulation site, by compensating for involuntary head movements.
In this way, operator fatigue is reduced, as clinicians are only required to supervise the process, and subject comfort improves, since patients are not asked to remain strictly immobile during the TMS session [42], [44], [45].
Furthermore, these systems regulate the interaction force between the coil and the scalp to provide the optimal contact without excessive pressure [46], [47], [48], [49], [50], [51]. This results in TMS procedures more tolerable and in which the clinical drop out is reduced [52].
From an operational perspective, automation in TMS can streamline the clinical workflow. In particular, the possibility of pre-programmed stimulation protocols reduces overall procedure time, improving operational efficiency and decreasing the need for continuous clinician training.
Automation can lower practical barriers to TMS treatment, broaden and support its widespread adoption. Treatment can become more economically sustainable, by minimizing reliance on highly specialized personnel [53],

[54], [55]. Although human supervision remains necessary, a single operator can manage multiple robotic systems simultaneously.

2.2 Robot-Aided TMS Platforms

After outlining the limitations of conventional TMS administration and the advantages introduced by automation, the following section describes robot-aided TMS platforms, detailing their structure, the main categories currently available, and the related technical requirements.

A robot-aided TMS platform is composed of a robotic manipulator, a neuronavigation software with its stereotaxic system, a TMS stimulator with its coil and a central workstation for real-time control and data processing (Fig. 2.2). The robotic manipulator places and holds the coil over the subject's scalp by continuously compensating for head movements in order to maintain an accurate alignment with the target stimulation site. To monitor in real-time head and coil movements a low-latency and high-precision camera system is placed to cover the robot working space. Passive reflective markers, attached both to the patient's head (usually through a headband) and to the coil, enable the cameras to continuously track their position and orientation. Neuronavigation is based on a stereotaxic system and a dedicated software that reconstructs high-resolution anatomical models of the subject's scalp and brain by co-registering head geometry data with magnetic resonance imaging (MRI) scans. Neuronavigation assists operators in the accurate localization of the stimulation target and enables continuous monitoring and recording of the position and orientation of the coil relative to the patient's head [56], [57].
The software running on the control workstation integrates information from the robot sensors, models of the subject's scalp and brain, and optical inputs.

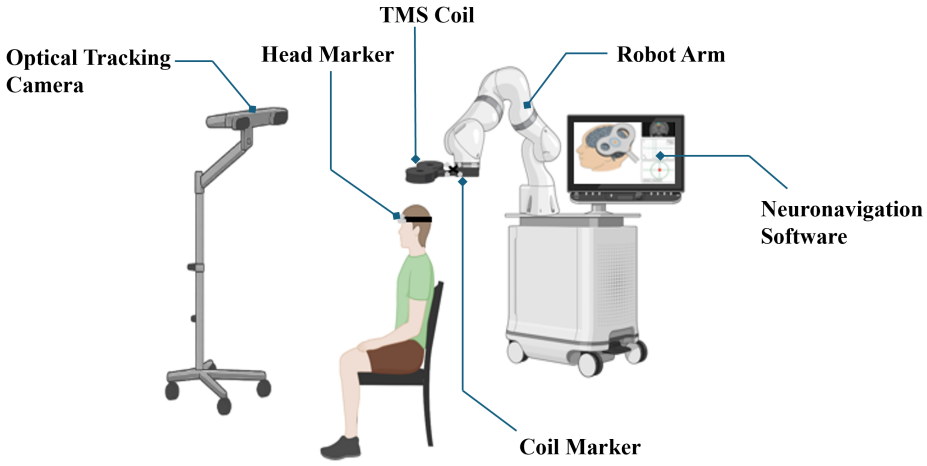

Fig. 2.2 In a standard robot-aided TMS procedure, the participant is seated comfortably in a chair. A high-precision optical camera system is positioned to cover the robot's workspace, enabling real-time monitoring of any movement of the head and coil during the session. The head and the coil are tracked by the camera thanks to passive markers placed on them. The coil's actual position and orientation relative to the stimulation target on the participant's head are visualized on the monitor via the neuronavigation software.

Through this closed-loop architecture, the system can continuous control the adjustments to the coil pose, even during subject head motion.

2.2.1 Robot-Aided TMS Platform Classification

Robot-aided TMS platforms can be classified into two main groups: ad-hoc systems and adapted systems. The former includes fully customized systems, with hardware and software components designed exclusively for TMS application. The latter, on the other hand, consists of modular systems which integrate commercial components, such as robotic arms originally developed for other purposes, neuronavigation systems and TMS devices, into a unified system.

Ad Hoc Platforms

A representative example is the commercial solution Axilum Robotics TMS Robot, which integrates a seven-degrees-of-freedom (DoF) robotic arm with a two-DoF chair designed to place the subject's head at the center of the platform hemispherical workspace. This configuration enables access to all cortical targets, including the occipital cortex, without the need to reposition the patient.

The spherical kinematics of the arm, together with a specialized robotic wrist designed to rotate around a fixed point at the coil–scalp interface (remote center of rotation), allow the coil to follow the curvature of the head while maintaining a tangential orientation at each stimulation site [49], [58]. Through this design the occurrence of critical configurations (singularities) is minimized, and movements around the head are smooth, safe, and continuous. Furthermore, the platform implements a control system that adjusts the coil position and orientation according to real-time target coordinates and head tracking data to maintain constant coil alignment with the target site throughout the procedure [49]. In addition, the adjustment of the contact coil-to-scalp force, detected by sensors embedded in the coil, further contributes to stimulation stability and subject comfort [49].

Despite its accuracy [59] and reliability [60], [61], the system faces practical barriers to widespread adoption. Due to its size (1950 mm × 1523 mm × 769 mm) and weight (~400 kg), it requires a dedicated installation space, which is often unavailable in standard clinical environments. Limited portability also complicates the possibility of sharing the system across facilities. Additionally, coil compatibility is restricted to a specific set of supported models, which constrain flexibility for clinical and research centers that employ different stimulation protocols and coil geometries.

Some years later, a more compact six-DoF robotic platform was introduced for research and preliminary clinical evaluation [34], [62]. This platform

moves the coil around the head following the same hemispherical workspace principle described for the previous platform, but with a simpler mechanical structure [34], [62]. In this configuration, the robotic wrist has a conventional kinematic structure: it can tilt and rotate the coil in various directions, but it is not designed to keep the contact point fixed when the angle changes. Therefore, when the coil orientation is adjusted, the point of contact may shift slightly from its original position. To preserve space accuracy, the robot automatically compensates for this displacement through coordinated movements of the other arm joints.

The system is controlled in position and achieves spatial accuracy comparable to that of the Axilum Robotics TMS Robot (positional error < 1 mm; angular error < 1°) [34]. However, the absence of active force regulation may result in greater variability of contact pressure during unwanted patient's head movements, affecting the comfort and the safety during the stimulation procedure. Moreover, the system remains at an early clinical stage of development, having been tested only in a pilot study in the treatment of depression [34]. Larger clinical validation studies will be necessary before it can be considered for routine clinical use.

Adapted Platforms

An early approach to modular systems for robot-aided TMS platforms involved adapting a neurosurgical robot equipped with a dedicated software for procedure management [63]. The system integrated a custom software to process MRI images, reconstruct the scalp surface, and finally register it to a set of manually acquired 3D coordinates.

Although the paltform achieved a positional accuracy of approximately 2 mm and an angular error of around 1° [63], the absence of a real-time tracking system and contact feedback required the patient to remain immobilized to ensure safe operation.

Some years later, robot-aided TMS systems evolved integrating industrial robotic arms with MRI-guided neuronavigation softwares and optical tracking systems [51], [64], [65], [66], [67], [68]. A major improvement over earlier designs was the introduction of real-time head motion compensation, which eliminated the need for rigid head fixation while maintaining precision and enhancing patient comfort. Performance assessments generally reported positional errors within 5 mm and angular errors less than 3.5°. Initially, the development of these platforms was mainly directed toward improving their spatial accuracy, while the force parameter between coil and scalp was not yet monitored. Only later, understanding its relevance for patient safety and comfort, the platforms started to incorporate force sensors and coil–scalp contact regulation strategies into the control system design [48], [51], [66], [67].

However, industrial robotic arms can present critical issues when applied in a TMS application. During a TMS procedure, the operational workspace is limited to the upper part of patient's body, mainly around the head, while industrial robots are designed to operate across much larger work envelopes. This design discrepancy can lead to unnecessary motion complexity and to a reduction of the system accuracy. Industrial robots, moreover, are equipped with high-power actuators optimized for speed and payload capacity. While these technical features are advantageous in industrial applications, they can arise safety concerns in clinical environments, where patient comfort, and safe patient and operator interactions are mandatory requirements.

These constraints have driven a transition toward collaborative robots, or cobots, which, combining low-inertia structures with force-limited actuation, are specifically designed for safe, close-proximity interaction with humans. Consequently, recent developments in robot-aided TMS have begun to exploit cobot technology, adapting both hardware and control architectures to meet the specific requirements of TMS [46], [47], [50], [69].

Most of these systems are still at a research-prototype stage, and the most

representative examples are analyzed below.

One proposed platform, developed to achieve high positioning accuracy, integrates a seven-DoF collaborative robot (Panda by Franka Emika GmbH) with a commercial neuronavigation system (SofTaxic Optic by E.M.S. srl) [46], [69]. A dedicated alignment procedure between the robotic arm and the tracking system was specifically designed for the spherical space around the head.

This platform achieves positioning errors of approximately 2 mm and angular deviations below 2° [46].

However, the alignment procedure is time-consuming and requires both the cameras and the robot base to remain perfectly stationary throughout the TMS session. In practice, the cameras are often susceptible to inadvertent movements or may need to be repositioned to meet field-of-view requirements. In either case, the calibration is disrupted, and the entire procedure must be repeated.

Another experimental approach employs a six-DoF collaborative robot (UR5 by Universal Robots) integrates with an alternative tracking strategy [47]. Fiducial markers are mounted on a pair of AR (Augmented Reality) glasses worn by the subject and detected by a monocular camera.

Qualitative results suggest good tracking stability, although no explicit quantitative data on positioning or orientation errors are reported.

At this stage, the platform should be considered as a promising but still preliminary proof of concept. However, the integration of AR glasses opens interesting clinical perspectives, as it could enable robot-aided TMS to be combined with immersive augmented environments aimed at improving patient engagement and supporting interactive neurorehabilitation protocols.

A more recent research platform has addressed another important aspect of robotic TMS: the coil–head interaction. This system is composed by a six-DoF collaborative robot (UR5e by Universal Robots) and implements a hybrid position/force control adapted to an incurved coil geometry [50]. The curved

design increases the surface contact between the coil and the patient's head, improving mechanical stability and reducing the sensitivity of the stimulation to small head movements. However, the increased surface contact generates also higher friction which can result in slower coil repositioning.
Force control is dynamically scheduled: higher forces are briefly applied to rapidly correct positioning errors, then reduced to maintain a comfortable, steady contact. While this improves stability, the initial force peaks (>10 N) could raise safety concerns in a clinical setting if not precisely tuned.
While the system improves contact stability under controlled conditions, the reliance on force peaks, sensitivity to parameter tuning, indicate that further development is required to ensure safe, consistent operation and reproducible outcomes.
To date, the only commercial platform that can be classified as an adapted platform is TMS-Cobot (by Axilum Robotics). This collaborative robot, with six-DoF, is compatible with the main commercial neuronavigation systems. The system offers a positioning accuracy of less than 2 mm and is currently the only robot-aided TMS system for TMS to have both CE marking and FDA approval (Axilum Robotics, Schiltigheim, France). However, its workspace is half hemispherical. Due to the compact geometry and kinematic configuration of the arm, access to some occipital regions may be limited, which can slightly reduce the versatility of the system for protocols targeting more posterior areas.

Multi-locus TMS

Multi-locus TMS (mTMS) represents a sui generis solution, a hybrid between an ad-hoc and adapted platform.
The stimulation system, specifically designed for TMS, is composed of a multi-coil transducer (a planar array of five coils) powered by a multi-channel generator, which controls the currents in each coil and enables electronic

displacement and orientation of the cortical electric field without physical movement of the hardware.
Such a design allows rapid retargeting on the millisecond scale [70], [71] within a defined cortical area (~30 mm in diameter).
More recently, the relatively heavy coil-array system (~5 kg) has been integrated with a collaborative robot (Elfin 10; Han's Robot Co Ltd, China) to achieve more precise, stable positioning and to actively compensate for involuntary head motions [55].
However, the planar coil configuration restricts the controllable cortical area and fails to guarantee optimal contact in highly curved regions of the scalp. Furthermore, the simultaneous operation of multiple coils raises issues of heating and acoustic noise.
These technical constraints, combined with the need for specialized expertise and infrastructure, currently limit the system's implementation to a few advanced research and clinical centers.

2.2.2 Technical Requirements

Designing a robot-aided TMS involves translating clinical practice requirements into engineering specifications to ensure the procedure is both safe and therapeutically effective (Fig. 2.3).
Spatial accuracy is a main performance criterion: the system should place the coil relative to the cortical with a translational error of ≤ 3 mm and an angular deviation of $\leq 5°$ [34], [46], [49], [54], [68]. This level of accuracy should be maintained during the entire stimulation session, even when the patient moves involuntarily [42].
The contact force between the coil and the scalp should be monitored as it might affect both patient comfort and positional stability. The pressure should have minimal variability, with a standard deviation below 1 N and a range of 5-6 N [72]. This parameter should be actively controlled through

dynamic adjustments based on sensor feedback, and passively managed using lightweight, compliant mechanical solutions [47], [49], [50], [51].
From a mechanical and kinematic standpoint, the platform should be able to reach all cortical areas of interest, including lateral and posterior regions, without the need to reposition the patient [46], [49]. The kinematic design should avoid unstable or near-singular configurations, ensuring smooth, safe, and predictable movements throughout the workspace [73].
To operate safely, the platform should integrate multiple layers of collision-prevention measures by implementing hardware and software strategies. Real-time optical tracking of the head and coil pose should provide the control application with continuous feedback to guarantee coil does not approach sensitive facial areas. If head tracking is lost due to marker occlusion or if the head exceeds safety velocity limits, the system should immediately trigger an alarm and execute emergency procedures, such as retracting the coil along pre-defined safe paths and, if necessary, automatically shutting down [46]. Unexpected collisions should be detected through joint-level torque sensors to enable instantaneous motion interruption. Furthermore, emergency stop buttons located on both the robot base and the operator console must, when pressed, disable all actuators and engage mechanical brakes.
Finally, usability is a driver factor in clinical and research adoption. Usability of robot-aided TMS platforms should be improved simplifying the interaction between operator and system to make it more immediate and reliable, while reducing cognitive load and training time. The graphical user interface (GUI) should therefore be clear and consistent, guiding the operator through each step of the procedure without introducing unnecessary actions [74]. Limiting mandatory steps and interactions to 12–15 and ≤ 30, respectively, helps minimize distractions and reduce the number of errors [75]. Guided procedures and preconfigured protocols could reduce the need for highly specialized skills, allowing less experienced operators to safely conduct a session after a short supervised training period of 2-3 sessions.

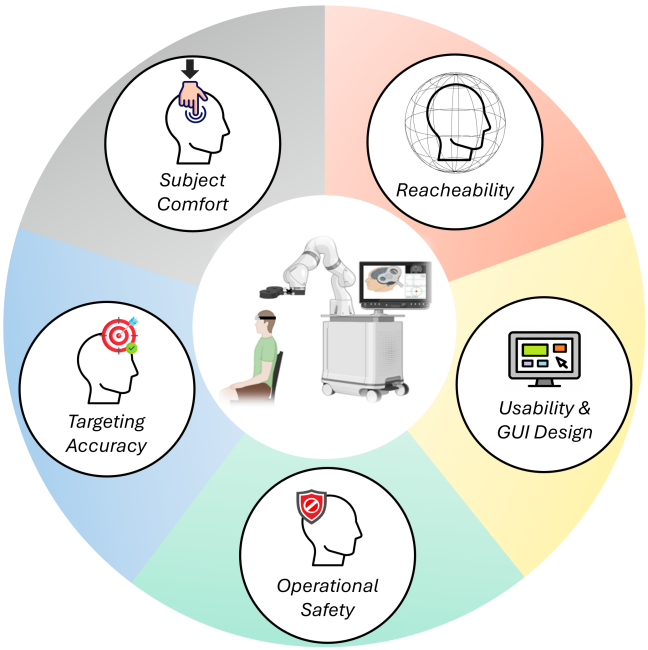

Fig. 2.3 Main design requirements for robot-aided TMS platforms.

2.3 Robot-Aided TMS Platforms in Clinical and Research Settings

The methodological advantages introduced by robot-aided TMS platforms become truly meaningful when they have a clinical or research impact. This section will examine the main clinical and research applications of this technology, starting with a general overview of TMS protocols and then focusing on robot-aided TMS motor mapping and robot-aided repetitive TMS (rTMS) protocols, where this technology is most commonly applied.

According to stimulation parameters and resulting effects, TMS can be classified into two main modalities: single-pulse TMS and repetitive TMS (rTMS) [76], [77].
Single-pulse TMS, typically administered at interstimulus intervals (ISI) of 4–8 s, is used for the assessment of cortical excitability and the investigation

of human brain function [77].
By contrast, rTMS involves repeated stimulus train that can induce effects persisting beyond the stimulation period. The direction and duration of rTMS effects are influenced by multiple parameters, such as the temporal structure of the stimulation trains, stimulation frequency, intensity, and the total number of pulses delivered. Conventionally, high-frequency rTMS ($\geq$ 5 Hz) facilitates cortical excitability, whereas low-frequency protocols ($\sim$1 Hz) are more often associated with inhibitory effects. Within established safety limits, increasing the intensity of stimulation and the the number of pulses is associated with a greater magnitude and persistence of rTMS-induced after-effects. However, the temporal organization of stimulation pattern, such as train duration and inter-train intervals, can produce robust and enduring neurophysiological changes even at lower stimulation intensities.
Clinical investigations of rTMS span diverse neuropsychiatric conditions, with the most established therapeutic evidence in major depressive disorder and ongoing evaluation in stroke, neuropathic pain, aphasia, and hemispatial neglect [78].

2.3.1 Robot-Aided TMS Motor Mapping

Motor mapping is a commonly used single-pulse TMS protocol in which stimulation sites are positioned on a regular spaced grid that covers the subject scalp.
To generate a posterior-anterior current in the underlying cortex, the coil is positioned tangentially to the scalp and oriented at around 45° to the sagittal plane. Typically, stimulation intensity is set at a fixed percentage above the individual resting motor threshold (commonly 110–120% RMT). The RMT is the minimum stimulation intensity needed to evoke MEPs of at least 50 μV in 50% of trials in a resting muscle. Single pulses are delivered generally with ISI of 4–8 s, while the target grid sites are stimulated sistematically.

Motor-evoked potentials (MEPs) recorded from contralateral muscles using surface electromyography are then used to identify the responsive sites of the map [79], [80].

Spatial accuracy largely determines the quality of cortical motor mapping: even small coil placement errors degrade the resolution of the resulting map. Motor-mapping protocols demand dense grids (5–7 mm spacing), precise control of coil placement, and high repeatability over hundreds of stimuli and across sessions. Robot aided TMS systems meet these requirements effectively. Indeed, a direct comparison shows that robot-aided TMS systems achieve smaller static errors and more consistent repositioning across sessions than manual placement, with average static errors around 3 mm compared to 6 mm for human operators and maximum intersession errors of ≤ 1.0 cm versus ≤ 2.4 cm [59]. These advantages are achieved without additional procedural burden, while lowering operator workload and maintaining participant comfort [59], [60], [81].

Mapping duration in robot-aided TMS reflects both the chosen protocol parameters and the technical capabilities of the robotic system. In a early study, where an industrial robot was repurposed for TMS, stringent safety constraints severely limited movement speed, so that even small maps (32–48 sites) required 30–50 minutes [82]. Later, the introduction of robot-aided TMS-built systems, has improved efficiency through optimized kinematics and smoother trajectories, making TMS mapping feasible in clinical contexts.

In current practice, robotic TMS mapping protocols allows the stimulation of 144 sites in about 40 minutes (ISI =4 s; 4 pulses per site).

To further improve tolerability, particularly in paediatric populations, accelerated protocols have also been explored, employing ISIs as short as 1 s that reduces the total time to 15 minutes in unilateral 144-site maps, with four stimuli delivered at each point [83]. Althoug these findings support the feasibility of implementing such accelerated protocols, an ISI of 1 second does not preclude the risk that very short intervals may induce unintended

plasticity-related effects.
A strategic refinement feasible with the robot-aided TMS system in this type of protocol could be the use of pseudorandom stimulation sequences. Instead of advancing systematically across the grid, stimulation sites can be selected so that consecutive pulses are delivered to non-adjacent locations. This may help dissociate short interstimulus intervals from repeated activation of nearby cortical regions, reducing the risk of local plasticity while preserving the efficiency of rapid mapping protocols.

2.3.2 Robot-Aided Repetitive TMS (rTMS)

Conventional repetitive TMS (rTMS) protocols last 20–30 minutes, during which the operator is asked to manually maintain the coil, which typically weighs 2–3 kg, fixed over the stimulation target. Such a condition is physically demanding and may lead to minor variations in coil placement relative to the stimulation site, hence reducing treatment efficacy. Robot-aided rTMS can address these issues offering greater stimulation stability, increased standardization and improved reliability of clinical outcomes.
These systems have been used to treat neuropathic pain [84], Tourette syndrome in pediatric populations [61], and major depressive disorder [34], [85]. They have also been employed to investigate higher-order cognitive functions, such as the mechanisms of language production [86], the role of the supplementary motor area (SMA) to executive control [87], and the neural basis of cognitive dissonance [88].
However, most studies have simply used robot-aided TMS as a methodological device, rather than evaluating its clinical or neurophysiological efficacy compared to manual administration. Therefore, clinical practice must consider whether the methodological advantages of robotic systems translate into therapeutic efficacy equivalent to or superior to that of standard TMS administration.

Nevertheless, preliminary evidence starts to address this question. For example, in the treatment of neuropathic pain, repeated robot-aided rTMS sessions have been associated with a reduction in pain that is both clinically meaningful and durable [84]. After three sessions, 43% of patients achieved at least 40% pain relief, which lasted for an average of 12 days. Among initial responders, 89% maintained this improvement after one year. These outcomes are broadly consistent with earlier non-robotic studies [77], although differences in stimulation parameters and different follow-up duration limit the strength of direct comparisons [84].

Robot-aided rTMS has also been evaluated in major depressive disorder, targeting the left dorsolateral prefrontal cortex (dlPFC) [34]. The pattern paradigm consisted of two-second trains followed by 28 seconds of rest for up to 20 minutes. Compared with manual application, robotic assistance reduced preparation time by 53% and improved positioning precision (initial error: 0.94 mm and 0.11° vs. 11.17 mm and 4.06°). Clinically, outcomes assessed with the Beck Depression Inventory-II and regional cerebral blood flow did not differ significantly between the two modalities, suggesting comparable outcomes.

2.4 Discussion and Conclusions

Although the development of automated TMS platforms represents a significant step forward compared to manual standard administration, the available evidence still provides only a partial picture. Most of the available studies focus mainly on evaluating the technical performance of these systems, neglecting their clinical effectiveness. The lack of multicentre clinical trials, standardized comparative analyses and follow-up data hinders an accurate assessment of the actual therapeutic efficacy, economic sustainability and acceptability of automated systems for TMS administration.

This discussion examines how far technical improvements translate into clinical benefits and outlines future directions aimed at bridging the gap between technological performance and therapeutic value.

The evolutionary trajectory of robot-aided TMS has moved so far toward systems that ensure accuracy and stability during wide head movements in active tasks, offer full cranial target coverage, maintain constant force and pose over prolonged sessions, enable more automated workflows and support personalisation based on anatomical and physiological data [34], [46], [49], [55], [71].

However, there is still no "ideal" robot-aided TMS platform.

Current solutions represent an advance over standard practice but remain fragmented: most optimise a subset of features while compromising others. As a result, advances tend to appear as isolated or experimental features rather than parts of a unified architecture.

Ad hoc and adapted platforms should be considered as solutions to different needs. Both are the result of design compromises: the former integrates kinematics, control systems and safety strategies natively developed for TMS. The latter, on the other hand, focus on flexibility, portability and the possibility of integration with existing devices.

Ad hoc systems offer the highest technical performance, but they are costly, bulky and not very versatile [34], [49]. Although these solutions function very well, they risk confining robotic TMS to a few specialized centers, failing to meet the objective of democratizing access to TMS.

Adapted systems provide flexibility and potential cost savings, but this advantage comes at the price of evident technological immaturity. Most are research prototypes, whose results are preliminary and often show insufficient quantitative validation [47], [50].

The mTMS platform represents the most innovative approach, shifting the problem of automation from physical coil positioning to coil electronic field regulation [70], [71]. However, the system is very heavy (~5 kg), so it re-

quires a robotic support during the TMS procedure [55]. This technological complexity inherently restricts its use to highly specialized operators.

Although the automation of TMS systems is rapidly evolving and has generated innovative engineering solutions, their clinical maturity and economic and operational sustainability remain limited. The transition from engineering innovation to therapeutic value depends on demonstrating efficacy and reproducibility in clinical practice. The absence of large-scale multicenter studies therefore constitutes the major barrier to the development of standardized protocols and evidence-based recommendations.

In the few studies available, these platforms has been shown to improve the accuracy and spatial resolution of cortical representations and to provide reliable results across sessions [60], [89], [90].

Furthermore, they have demonstrated clinical efficacy comparable to human operators, with similar clinical outcomes reported in neuropathy [77], [84] and depression [34]. Due to these protocols require multiple sessions over several months, robot-aided TMS can help reduce inter-operator variability in treatment delivery.

The comparative study of major depression is significant [34]: although the robotic system is approximately ten times more accurate than manual administration, the clinical outcomes are only comparable. This suggests that other factors may be as important as the accuracy of coil placement to determine the clinical outcomes.

While this does not decrease the value of automation, it does highlight that simply replicating existing manual protocols through robotic platforms may not fully exploit the potential of these technologies.

It is necessary to design stimulation paradigms that take full advantage of robotic platforms. Such paradigms might include, for instance, dynamic protocols that adapt in real time to patient movements or spatially complex stimulation sequences targeting multiple cortical areas with temporally precise patterns, approaches that would be impossible to achieve manually.

Concurrently, advanced personalization algorithms should be developed to modulate stimulation parameters based on each patient's individual characteristics, thereby facilitating interventions that explicitly account for inter-individual variability.
Finally, the clinical and technological impact of robot-aided TMS should be considered within a broader context of healthcare and economic transformation, where the demand for non-invasive solutions is rapidly increasing. The global TMS market is expected to reach €2.3 billion by 2030. This trend reflects the growing demand for alternatives to pharmacological drugs and is driven by supportive health policies in Europe and the United States, increased investments in neurological care and research, and greater acceptance of TMS for patients who do not respond to standard therapies.
Therefore, robot-aided TMS can be considered as a tangible solution to improve clinical practice and accelerate research. By offering highly accurate, reproducible, and customized stimulation, it can enhance the effectiveness and operational efficiency of treatment, shorten sessions, decrease dependence on highly specialized personnel, and facilitate the investigation of complex neural mechanisms and pathological processes. The challenge ahead requires a paradigm change that moves the focus from technical performance to demonstration of effectiveness in a clinical or research context. This shift should prioritize robustness, ease of use, and economic sustainability in a design that is finally focused on the end clinical user and the patient.

In conclusion, this chapter provides the theoretical and technological background required to frame the experimental studies presented in the following chapters, all aimed at improving the precision and personalization of TMS.

Chapter 3

From Technological Designing to Neuroscientific Application: Experimental Studies with a Robot-Aided TMS Platform

3.1 Rationale

The core of this thesis is composed of three experimental studies which, while pursuing distinct scientific objectives, share a clear and consistent methodological thread: the use of robot-aided TMS platform in advanced TMS protocols. In each study, the robot-aided TMS platform is not only a technological support, but an advanced methodological tool for overcoming some of the limitations of manual TMS administration and for enabling stimulation protocols that were so far hard to achieve.

The first study has an engineering and developmental nature: it addresses the optimization and validation of an in-house robot-aided TMS platform. In this case, the robotic technology represents the object of investigation itself. The aim of the study focuses on the implementation of different control strategies designed to achieve accurate coil positioning and orientation and ensure safe

coil-scalp interaction. Unlike to manual administration, robot-aided TMS platform can actively compensate in real-time for the movements of the subject's head, maintaining a constant spatial targeting of the interest cortical region. This feature could be exploited by implementing innovative dynamic stimulation protocols, which can be administered while a subject performs complex movements.
The second study uses the previously validated robot-aided TMS platform to implement a rTMS protocol to investigate if it is possible selectively modulate direction-specific neuronal populations within the primary motor cortex (M1) during movement preparation. In the experimental design, the robotic platform allows for rapid and accurate repositioning of the coil between spatially distinct cortical sites (approximately 5 cm apart) within a time window of less than two seconds, achieving spatial precision and temporal efficiency impossible to reproduce manually.
The third study represents the most advanced stage of this methodological progression and combines a robotic platform with a real-time EEG-informed TMS algorithm. In this stimulation paradigm, each TMS pulse is delivered in synchrony with specific phases of the sensorimotor mu rhythm in order to investigate the effects of state-dependent stimulation on corticospinal excitability. The stability provided by the robotic system eliminates most of the source of spatial variability during the experimental TMS session. Such a level of control would not be achievable with manual administration because it could not guarantee the coil stability and spatial accuracy necessary to validate the state-dependent effect.

The following sections will describe in detail each of these studies, outlining their specific objectives, experimental designs, and main results.

3.2 Optimized Robot-Aided Transcranial Magnetic Stimulation (TMS) Platform: Evaluation of Control Approaches for Head Motion Compensation

The employment of robotic platforms in TMS applications could have a significant impact in the field of neuroscience, promoting the development of innovative TMS protocols.
For instance, the administration of TMS while subjects are engaged in complex motor tasks, such as walking, offers the possibility to investigate neural plasticity and sensorimotor integration in dynamic contexts that reflect real-life situations, in contrast to traditional TMS studies conducted under static conditions. This TMS application could have important clinical implications, especially in neurological conditions characterized by impaired gait control (such as Parkinson's disease, post-stroke gait deficits, and multiple sclerosis) in which stimulation delivering during gait could allow the modulation of neural circuits while they are functionally active, potentially enhancing the state-dependent plasticity and the specificity of the induced effects.
However, applying TMS while walking raises significant safety and accuracy challenges. To ensure consistent stimulation and effectively compensate for complex head movements, reliable and precise control strategies are needed.
Recently, an advanced robot-aided TMS system was developed [46], and it integrates a 7-degrees-of-freedom (DoF) robotic manipulator (Panda by Franka Emika GmbH), Polaris Vicra infrared cameras (by Northern Digital Inc.) and a SofTaxic neuronavigation system (by E.M.S. srl).
The platform, validated during real TMS sessions, implements an impedance control strategy to place the coil on the scalp and to compensate for head movements and an innovative hand-eye and robot-world calibration approach, specifically developed for TMS applications [69].
Here, to favor the accessibility and widespread application of robotic TMS systems, we present a refined version of the above-mentioned TMS platform

that incorporates an affordable, high-performance tracking system (Optitrack 13W, NaturalPoint Inc.) and the open-source neuronavigation software NeuRoRoNav [91].
On this improved platform, in order to advance the development of dynamic TMS protocols, we implement and compare four different control strategies for head motion compensation (high-stiffness isotropic impedance control, low-stiffness isotropic impedance control, selective impedance control and hybrid force-position control) to determine the most effective control approach for ensuring precise, consistent, and safe TMS application in both static and dynamic conditions. We evaluate which control approach offers the best performance in terms of tracking accuracy and contact force under identical experimental conditions, simulating simple translational and rotational head movements but also more complex head movements occurring during walking on traedmill.

3.2.1 Methods

Experimental Setup

In our experimental setup, two 7-DoF robotic manipulators (Panda, Franka Emika GmbH) are employed. One of them is used to hold a mock-up head and simulate both simple (translations and rotations) and more complex head movements (oscillations during treadmill walking); while, the other one places and moves the stimulation coil (D70 Alpha Coil, figure of eight, Magstim Co Ltd) on the subject's head, in correspondence to the stimulation site, compensating for simulated head movement.
The robots are equipped with torque sensors in each joint and its controller runs at a frequency of 1 kHz.
The two robots are fixed to a heavy metallic bench at a distance of one meter apart and custom 3D-printed adaptors are used in both cases to attach the dummy head and the coil to their respective end-effector.

The tracking system is composed by two Optitrack 13W infrared cameras (NaturalPoint Inc.) that track the position and orientation (i.e. the pose) of passive reflective markers.
The neuronavigation software employed is based on the open-source neuronavigator NeuRRonav developed by the NeuRRo Lab of the University of Michigan Medical School with the game engine Unity in C# [91].

Communication

The two infrared 13W Optitrack cameras (NaturalPoint, Inc.) track the head and coil that are both equipped with passive reflective markers. Thanks to ethernet cables, the cameras are connected to and powered by a Power-over-Ethernet (PoE) switch (Netgear Inc.) in turn connected to a Windows PC. Camera data captured is live-streamed to the Optitrack Motive software (NaturalPoint, Inc.), where rigid bodies' pose relative to the cameras' reference frame is computed and sent in real-time to the neuronavigation software.
The latter, developed in C# on Unity (2018.3.3f1) and adapted from the open-source TMS neuronavigation software NeuRRoNav [91], runs on the same Windows PC and receives the tracking information through the Optitrack Unity Plugin (version 1.1.0).
The robot control application has been implemented in C++ language using Qt libraries and runs on a Linux computer (OS Ubuntu 20.04 LTS). To send in real-time the poses of the head and selected hotspot for stimulation from the neuronavigator to the robot control application, we developed a UDP communication between both computers. Finally, the robot control application sends torque commands to the robot controller through TCP/IP protocol (Fig. 3.1).

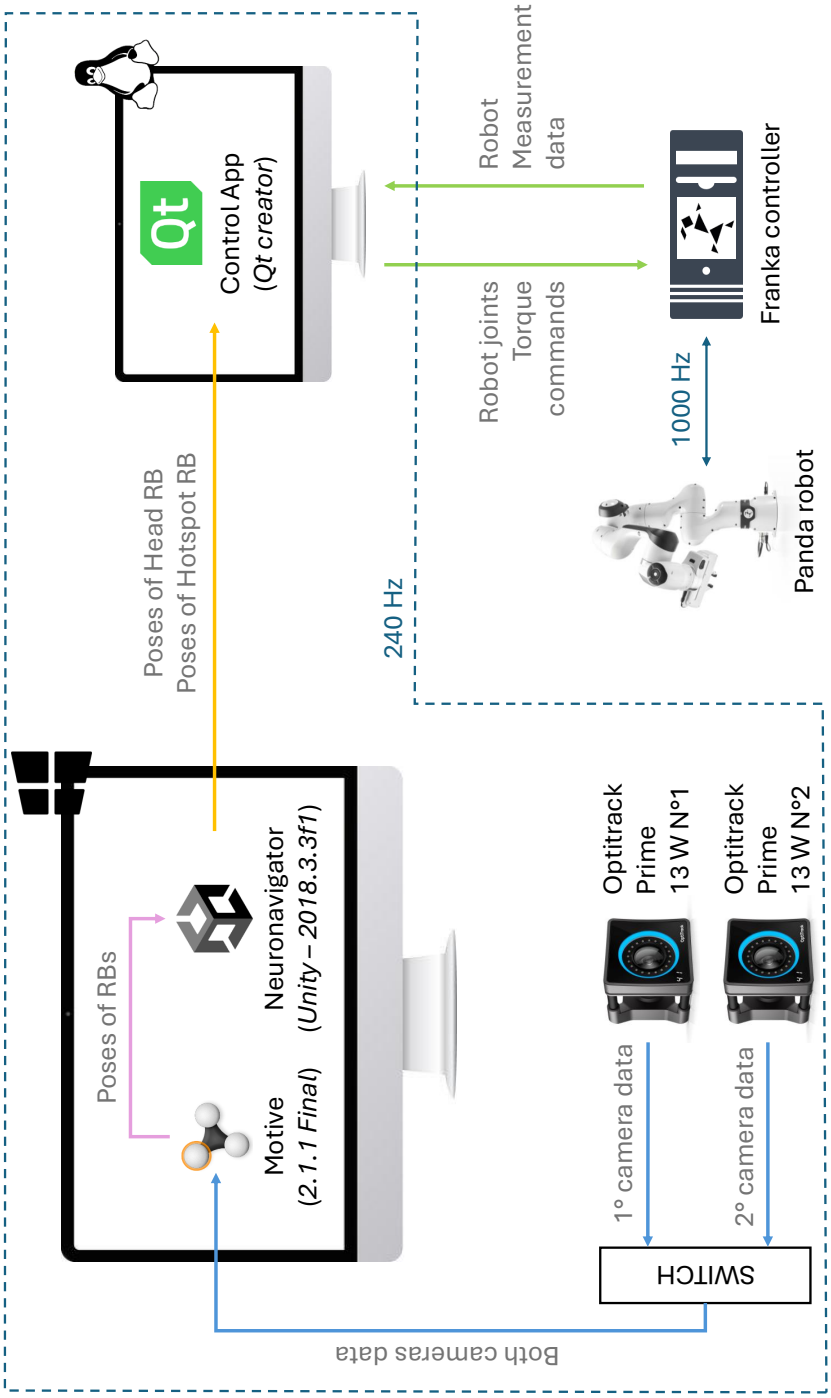

Fig. 3.1 Communications and data flow within the robot-aided TMS platform.

Neuronavigation and Calibration Protocol

Tracking System. As a first step, the Optitrack cameras require calibration in order to set their workspace and reference frame within Motive software. This is achieved by utilising the Optitrack CW-500 Calibration Wand, which is waved throughout the workspace until a sufficient volume is covered. At least 40,000 sample points must be registered for each camera to ensure the calibration is as accurate as possible.
Subsequently, the workspace reference frame is established by positioning the Optitrack CS-200 Calibration Square in the desired orientation. In this study, the xz-plane is horizontal,the z-axis runs parallel to the alignment of the robots, extending from the robot simulating head movements toward the robot holding the TMS coil, the x-axis is perpendicular to the z-axis and extends from the robots towards the cameras, and the y axis is vertical and points upward (Fig. 3.2).

Neuronavigator Software. The neuronavigation software NeuRRonav is a graphical user interface integrating motion capture that enables to visualize on a computer screen the virtual model of the subject's head and of the TMS coil as well as their respective poses in the workspace (Fig. 3.3).
Once the cameras and their workspace have been calibrated, the real tools (i.e., calibration tool, stylus, head marker and a coil marker), equipped with reflective markers and tracked in the Motive system, have to be calibrated and aligned with their virtual copy defined in the neuronavigation software.
The first step consists in calibrating the stylus length into the neuronavigator by placing its tip at the center of the calibration tool. The motion tracking system communicates to the neuronavigation software the orientation and length of the stylus' rod with respect to the optical markers placed on its handle. With this information the neuronavigator can recreate the exact virtual model of the stylus and replicate in real time its pose in the virtual environment. The

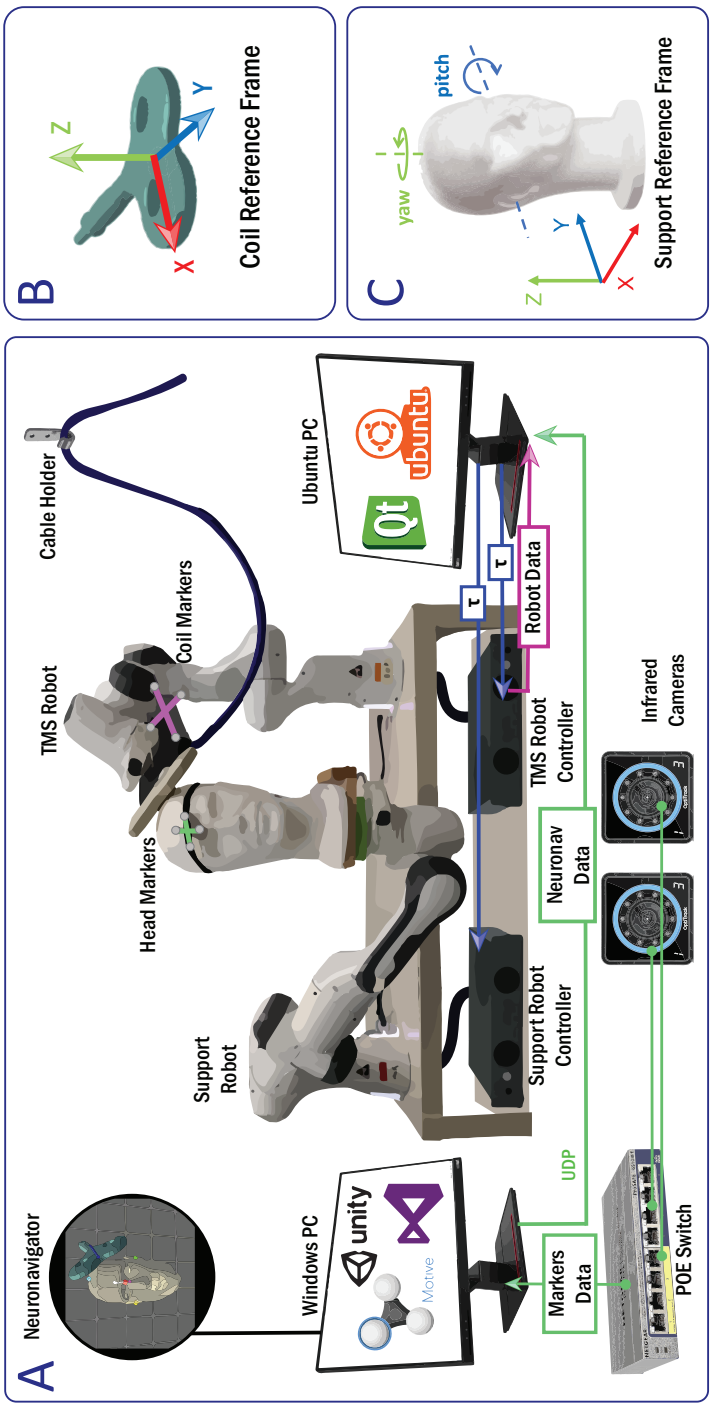

Fig. 3.2 Panel A: Experimental setup. Panel B: Coil reference frame with z-axis along the stimulation direction and x- and y-axes defining the stimulation plane on which the position error is computed. Coil frame is centered in the focal point of the magnetic stimulation field, at the centre of the two wings. Panel C: Support reference frame used to define directions of translation and rotation of the head.

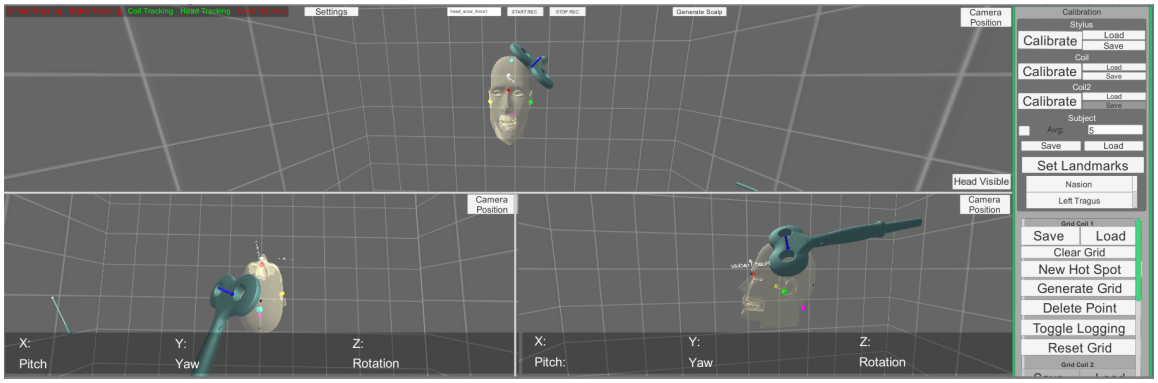

Fig. 3.3 NeuRRonav software graphical user interface after calibration.

next step involves calibrating the virtual model of the TMS coil. To do so, we place the tip of the stylus at the center, top and right extremities of the coil's stimulation surface. The neuronavigator uses these points to create the coil's virtual model and to define its pose with respect to the pose of the real coil's marker so that the neuronavigator can replicate in real time the movement of the real coil on the virtual one.

The final step of the calibration consists in creating the virtual model of the subject's head. We attach firmly the head marker on the subject's forehead, then we successively place the tip of the stylus on five fiducial points of the subject's head (inion, right tragus, left tragus, nasion, vertex). In this way, we communicate the relative position of the fiducial points with respect to the head marker to the software which then fits a generic virtual head model to the subject's head proportions.

The original open-source neuronavigation software NeuRRoNav [91] has been modified by implementing a UDP communication protocol that allows real-time transmission of the coil, head and hotspot poses to the robot control application. This solution provides synchronized tracking and correct operation of the robotic manipulator without requiring a specific middleware between the two softwares. In contrast, the previous platform configuration [46] relied on the commercial neuronavigation software SofTaxic. This software is proprietary and compatible only with NDI Polaris Vicra (Northern

Digital Inc.) tracking systems. Consequently, the former system was less flexible, costly, and offered lower performance. The refined platform employs the open-source NeurRRoNav software, which can be easily adapted to different types of tracking cameras, including the OptiTrack system currently in use.

Robot-camera calibration. At this stage, the robot-camera calibration, also known as tool-flange and robot-world calibration, is performed. The robotic manipulator places the coil in different poses which are captured by both the camera and the robot system [69]. The objective of this procedure is to set a common reference frame for all the components of the platform (robot, coil, and camera system). This is achieved by computing the transformation matrix between the reference frame of the cameras and the reference frame of the TMS robot, as well as the transformation matrix between the robot end-effector frame and the coil reference frame.

Hotspot. To define the stimulation hotspot, the robot is controlled in zero-torque mode (i.e., it has a transparent behaviour), allowing the operator to easily move it and place the coil on the desired stimulation point. Once positioned, a "target" virtual object relative to the head is created in the neuronavigation software at the current position of the coil's focus point.
During the validation of the four different control strategies, the same stimulation targets were used: three different robot configurations were evaluated by positioning the coil tangent to the dummy's scalp, i) aligned with the sagittal line and ii) approximately 5 cm lateral to the vertex toward the left hemisphere, with the handle oriented at +45° relative to the sagittal plane; and iii) approximately 5 cm lateral to the vertex toward the right hemisphere, with the handle oriented at -45° relative to the sagittal plane. These hotspot positions correspond to a stimulation at the vertex and a stimulation of the left and right primary motor areas, respectively.

TMS robot control approaches

The control algorithm of the robot-aided TMS aims to move the coil on the scalp and to keep it on the hotspot maintaining a correct position and orientation while compensating for head movements. Besides pose tracking to ensure high stimulation accuracy, the system must guarantee subjects' safety, limiting the contact force between coil and scalp.
We implemented four different control approaches: high-stiffness isotropic impedance control, low-stiffness isotropic impedance control, selective impedance control and hybrid position-force control.
All the numerical parameters (e.g., stiffness, damping, and target force values) used to implement the four different control strategies were derived from preliminary experimental trials.

Impedance control. Impedance control allows to maintain the coil on the hotspot, without a direct regulation of the contact force but adjusting the impedance between the robot and the environment [92].
Commanded joint torques are computed according to the following equation:

$$\tau = J^T[K(x_d - x) - D(J\dot{q})] + C\dot{q} + G, \tag{3.1}$$

with τ being the 7x1 joint torque vector and J the 6x7 Jacobian relative to the robot base frame; x_d and x the desired and current end-effector pose expressed as 6x1 vectors in the Cartesian space, with respect to the robot base frame. $\dot{q}$ is the 7x1 joint velocities vector. K and D are respectively the stiffness and damping 6x6 matrices. C is the contribution of the centrifugal and Coriolis torques and G is the 7x1 gravity torque vector. Furher details on the definition of x_d relative to the stimulation target can be found in [46].

High-stiffness and low-stiffness isotropic impedance control. In the first approach, the impedance is isotropic i.e., the same in each direction. K and D are defined as:

$$K_{isotropic} = diag(K_t, K_t, K_t, K_r, K_r, K_r)\,,$$
$$D_{isotropic} = diag(D_t, D_t, D_t, D_r, D_r, D_r)\,, \quad (3.2)$$

with $K_t = 2500$ N/m for high stiffness value or $K_t = 1500$ N/m for low stiffness value, $K_r = 50$ N/rad, $D_t = \sqrt{K_t}$ Ns/m and $D_r = \sqrt{K_r}$ Ns/rad.

Selective impedance control. The second approach employs a anisotropic impedance control that selectively reduces the impedance value along the stimulation direction, i.e., the direction of contact between the coil and the scalp. This approach aims to increase safety and comfort (through a compliant coil behaviour towards the head) while maintaining high accuracy in the coil positioning (stiff coil behaviour in orientation and position on the stimulation plane). In this case, the stiffness and damping matrices in 3.1 are defined as:

$$K_{selective} = diag(K_t, K_t, K_z, K_r, K_r, K_r)\,,$$
$$D_{selective} = diag(D_t, D_t, D_z, D_r, D_r, D_r)\,, \quad (3.3)$$

where $K_z < K_t$, being z the stimulation direction relative to the coil reference frame (see Fig. 3.2 B). In the experimental validation the following values were employed: $K_t = 2500$ N/m, $K_z = 1500$ N/m, $K_r = 50$ N/rad, $D_{t|z} = \sqrt{K_{t|z}}$ Ns/m and $D_r = \sqrt{K_r}$ Ns/rad.

Hybrid force-position control. The hybrid force-position approach decomposes the task space into unconstrained directions along which the system is controlled in position and constrained directions where it is controlled in force

[93], [94]. Position control is used to place the coil on the target area with high accuracy, compensating for head movements, while force control is designed to regulate and maintain the force applied along the normal direction of the scalp [49]. To avoid stability problems of the force control during clear non-contact situations we first move the coil to the desired position with the isotropic impedance control described earlier. Once the robot has reached the desired position on the scalp, it switches to the hybrid force-position control. A target normal force is then applied to ensure consistent coil-to-scalp contact [72]. The nominal target force was set to $5\,N$ in testing trials involving head rotations and simulated walking, while for translational movements, a slightly higher force value $6N$ was employed to compensate minor inertial interactions between the coil and its cable.
The hybrid control commands the torques of each joint according to the following equation:

$$\tau = J^T[\Omega(K(x_d - x) - D(J\dot{q})) + \overline{\Omega}(F_d + K_f(F_d - F_s) - K_{vf}(J\dot{q}))] + C\dot{q} + G, \quad (3.4)$$

where Ω and $\overline{\Omega}$ select the directions along which the robot is controlled in position (xy plane in the coil reference frame as depicted in Fig. 3.2 B) and in force (the z-axis) and are defined as follows:

$$\Omega = \begin{bmatrix} R_c S_t {}^bR_c^T & 0 \\ 0 & {}^bR_c S_r {}^bR_c^T \end{bmatrix}; \quad \overline{\Omega} = \begin{bmatrix} {}^bR_c(I - S_t){}^bR_c^T & 0 \\ 0 & {}^bR_c(I - S_r){}^bR_c^T \end{bmatrix} \quad (3.5)$$

with ${}^{b}R_{c}$ the rotation matrix from the robot base to the coil reference frame, I the 3x3 identity matrix and S_t and S_r respectively the 3x3 translation and rotation selective matrix expressed in the coil reference frame (Fig.3.2 B). In particular $S_t = diag(1,1,0)$ and $S_r = diag(1,1,1)$, with non-zero elements on the direction to be controlled in position and zero elements on the direction to be controlled in force.
Referring to Eq. 3.4, F_d and F_s are respectively the desired and the actual 6x1 force vectors at the coil, expressed in the robot base frame; F_s is collected using the FCI libraries and estimated from the torque sensors embedded into each robot joint. $K_f = 0.9$ and $K_{vf} = 0.2$ Ns/m represent respectively the proportional and derivative control gains of the controller in the force-controlled direction. F_d is defined as follows:

$$F_d = Ad^T \cdot {}^{c}F_d \tag{3.6}$$

with ${}^{c}F_d = [0,0,5,0,0,0]^T$ N the desired force with respect to the coil frame and Ad the adjoint matrix needed to express the desired interaction at the coil with respect to the base reference frame. Ad is defined as:

$$Ad = \begin{bmatrix} {}^{c}R_b & \hat{p} \cdot {}^{c}R_b \\ 0 & {}^{c}R_b \end{bmatrix} \tag{3.7}$$

with ${}^{c}R_b$ and p being respectively the rotation matrix from the coil reference frame to the robot base reference frame and the position vector of the robot base reference frame expressed in the coil frame. $\hat{p}$ and p are defined as follows:

$$\hat{p} = \begin{bmatrix} 0 & -p_3 & p_2 \\ p_3 & 0 & -p_1 \\ -p_2 & p_1 & 0 \end{bmatrix}; \; p = \begin{bmatrix} p_1 \\ p_2 \\ p_3 \end{bmatrix} \tag{3.8}$$

3.2.2 Experimental Validation

Head motion simulation

The four control approaches were tested and assessed first simulating head movements while walking on a treadmill and then simulating simple head translational and rotational motion (See Table 3.1).
A first dynamical test was conducted simulating the head movement of a person walking on a treadmill [95]. The support robot was controlled to move the dummy head through sinusoidal-like trajectory defined by the following equations:

$$z_h(t) = z_h(0) + A_z sin(2\pi f_t t)\,, \tag{3.9}$$

$$R_h(t) = R_h(0) R_y(t) \tag{3.10}$$

with z_h and R_h the vertical position and orientation of the dummy head with respect to the support base frame (Fig. 3.2 C). $z_h(0)$ and $R_h(0)$ represent values at time $t = 0$, whereas R_y is the elementary rotation matrix around the y-axis, here corresponding to the pitch direction, and computed as follows:

$$R_y = \begin{bmatrix} cos\theta & 0 & sin\theta \\ 0 & 1 & 0 \\ -sin\theta & 0 & cos\theta \end{bmatrix}, \tag{3.11}$$

$$\theta(t) = A_\theta sin(2\pi f_\theta t) \tag{3.12}$$

To simulate walking with slow velocity ($0.6\ m/s$), the translation and pitch amplitude were respectively set to $A_t = 10\ mm$ and $A_\theta = 2°$; whereas the frequency of vertical movements and pitch rotations were respectively set to $f_t = 1\ Hz$ and $f_\theta = 1\ Hz$ [95]. A total of 36 trials, each lasting 30 seconds, were collected for each control strategy.
The support robot moved the dummy head along each axis and along the diagonals of the XY, XZ, and YZ planes -one at a time- of the support reference

frame (Fig. 3.2 C). This was performed as a series of five translations, always starting from the same point. Control algorithms were tested for movements of 10 *mm* and 30 *mm* in both positive and negative directions, each one at the average velocity of 0.025 m/s, for a total of 72 different series of movements for each control approach [44].
A third test was performed for head rotations with an angular amplitude of 7°, simulating head yaw (Fig. 3.2 C), i.e., the "no" movement.
Five series of rotations were performed at an average velocity of $3°/s$ for a total of 12 different series of movements for each control approach.
Each series of movements, both for translations and rotations, is composed of 10 movements (5 back and 5 forth) separated in time by a 2s pause during which the head remained still.

Table 3.1 Summary of simulated head motion protocols used for experimental validation

Motion type	**Axes**	**Motion magnitude**	**Motion parameters**	**Trials**
Walking simulation	Z translation and pitch	10 mm (Z), 2° (pitch)	Frequency: 1 Hz	36 trials per control strategy, equally distributed across three hotspots (12 trials per hotspot).
Translational motion	X, Y, Z and XY,XZ, YZ diagonals	10 and 30 mm	Velocity: 0.025 m/s	72 trials per control strategy, equally distributed across six directions and three hotspots (12 trials per direction and 4 trials per hotspot).
Rotational motion	Yaw	7°	Velocity: 3°/s	12 trials per control strategy, equally distributed across three hotspots (4 trials per hotspot).

Data Analysis

Translational and rotational performance were evaluated under two experimental conditions: the static condition was defined as the 2 s pause intervals during which the head remained still, while the dynamic condition corresponded to the active phases of simulated head movements.
During simulated walking on treadmill, head motion performance was assessed exclusively under the dynamic condition.
Error in coil positioning is defined as the difference between the target coil pose (hotspot) and the actual coil pose.
The following measures were considered:

- Error in coil position: E_{xy}, the Cartesian norm of the positioning error in the stimulation plane, and E_z, the error along the stimulation axis.
- Error in coil orientation: E_ϕ, the orientation error norm in the SO(3) space.
- Normal interaction force: F_z the force between the stimulation coil and the mock-up head.

Before proceeding with the statistical analysis, outliers of the experimental trials were identified and removed (no more than 12% of trials were excluded per strategy) utilising the interquartile range (IQR) method [96].
A one-way analysis of variance (ANOVA) was employed to compare the performance of the four control strategies. When data did not meet normality assumptions (verified via the Shapiro-Wilk test), a one-way Kruskal-Wallis test was applied instead. The control approach was employed as a factor, and post-hoc comparisons were conducted using the Mann-Whitney test, with multiple comparisons corrected by Bonferroni.
For walking on treadmill movements, all parameters were evaluated using a one-way Kruskal-Wallis test. In this case, an additional analysis of the

variability (assessed through the standard deviation) of the above-mentioned indexes was conducted.
For translational movements, the same test was applied to all parameters, except for E_ϕ in both static and dynamic conditions, and for E_{xy} in dynamic conditions, which were analyzed using ANOVA.
Finally, for rotational movement, the one-way Kruskal-Wallis test was employed. The only exception was E_z in dynamic conditions, for which ANOVA was applied.

3.2.3 Results

Walking on treadmill

Statistically significant differences in coil positioning errors in the stimulation plane were identified among the various control strategies (Fig.3.4 A). The hybrid position-force control approach achieved lower errors compared to the selective ($p < 0.01$) and low-stiffness isotropic impedance strategies ($p < 0.01$), as well as the high-stiffness isotropic impedance control ($p < 0.05$). Furthermore, the selective control exhibited significantly reduced errors than the low-stiffness isotropic impedance control ($p < 0.01$). A similar trend emerged in the analysis of errors along the stimulation axis (Fig.3.4 B), where the hybrid control consistently outperformed all other approaches, resulting in significantly lower values ($p < 0.01$).
The orientation error also varied significantly across the control methods (Fig.3.4 C). The high-stiffness isotropic impedance control exhibited higher errors compared to the hybrid ($p < 0.01$) and low-stiffness isotropic impedance strategies ($p < 0.01$), whereas the selective control approach resulted in significantly lower values than the low-stiffness isotropic impedance approach ($p < 0.01$). The hybrid control showed a compact distribution around the desired force value ($5\,N$) (Fig.3.4 D), significantly higher than the impedance controls

(all p values < 0.01). Moreover, the high-stiffness isotropic impedance control exhibited higher interaction force values compared to both the selective ($p < 0.05$) and low-impedance controls ($p < 0.01$).

Subsequently, an analysis of the variability in coil positioning error, considering the stimulation plane, axis, and orientation, but also in the normal interaction force, was conducted to further assess the performance of each control strategy (Fig. 3.4 E-H). In the stimulation plane (Fig.3.4 E), the hybrid position-force control presented significantly lower error variation than all other strategies ($p < 0.01$), while the selective control exhibited reduced variability compared to the low ($p < 0.05$) and high-stiffness isotropic ($p < 0.01$) impedance controls.

Along the stimulation axis (Fig.3.4 F), the hybrid position-force control again showed the smallest error fluctuations compared to the other control strategies ($p < 0.01$).

In terms of orientation error (Fig.3.4 G), the hybrid position-force control strategy presented higher variability than the other control methods ($p < 0.01$). However, the orientation error variability remained below 1°, suggesting that despite statistical significance, the difference is not functionally relevant for the specific application.

Regarding the interaction force (Fig.3.4 H), the hybrid position-force control strategy resulted in significantly lower and more consistent force fluctuations compared to all other strategies ($p < 0.001$). Furthermore, the high-stiffness isotropic impedance control exhibited significantly higher force variation than both the low-stiffness isotropic ($p < 0.001$) and selective impedance control strategies ($p < 0.001$).

Translations

In dynamic conditions, coil positioning errors on the stimulation plane (Fig.3.5 A) were significantly lower for the low-stiffness isotropic impedance method

compared to the high-stiffness isotropic impedance ($p < 0.001$) and hybrid ($p < 0.001$) strategies. Regarding errors along the stimulation axis (Fig.3.5 B), the hybrid approach demonstrated significantly lower errors than all other strategies ($p < 0.01$).

However, the hybrid approach showed a greater orientation error (Fig. 3.5 C) compared to the high-stiffness isotropic impedance ($p < 0.05$), low-stiffness isotropic impedance ($p < 0.05$), and selective ($p < 0.01$) strategies.

Conversely examining the interaction force (Fig.3.5 D), the hybrid force-position strategy resulted in the narrowest distribution around the target value relative to all other control methods ($p < 0.01$).

Under static conditions, comparisons of control approaches in terms of coil positioning errors in the stimulation plane (Fig.3.6 A) showed that the low-stiffness isotropic impedance strategy achieved higher errors than both the high-stiffness isotropic impedance ($p < 0.01$) and hybrid position-force ($p < 0.01$) approaches. Additionally, the selective control strategy resulted in reduced errors compared to both the low-stiffness isotropic impedance ($p < 0.01$) and hybrid ($p < 0.01$) control approaches. When examining the error along the stimulation axis (Fig. 3.6 B), lower values are associated with the hybrid control than all other strategies ($p < 0.01$). Orientation errors (Fig.3.6 C) were, instead, higher in the hybrid control compared to the high-stiffness isotropic ($p < 0.01$), low-stiffness isotropic ($p < 0.05$), and selective ($p < 0.05$) impedance approaches. While the observed discrepancy is statistically significant, it is minimal in practical terms for the intended application.

The hybrid force-position control maintained a stable force profile (Fig.3.6 D) with values close to the target value and significantly lower variability than the other approaches ($p < 0.01$).

Rotations

Under dynamic conditions for traslational movements, no meaningful statistical differences were detected in coil positioning errors on the stimulation plane (Fig. 3.5 E) or along the stimulation axis (Fig.3.5 F) across the tested control methods. Similar to what is observed under static conditions, the orientation error (Fig. 3.5 G) demonstrated significant differences between the hybrid control and all other strategies ($p < 0.01$). Furthermore, the normal interaction force variability (Fig. 3.5 H) remained significantly different between the hybrid strategy and the alternative control methods ($p < 0.01$).
In static conditions, coil positioning errors on both the stimulation plane (Fig.3.6 E) and axis (Fig.3.6 F) did not show any statistically significant variation among the different control strategies. In contrast, orientation error (Fig.3.6 G) revealed a significant distinction only between the high isotropic impedance control and the hybrid force-position strategy ($p < 0.05$). In terms of interaction force (Fig.3.6 H), the hybrid control demonstrated significant differences compared to the high-stiffness isotropic impedance ($p < 0.01$), low-stiffness isotropic impedance ($p < 0.01$), and selective ($p < 0.01$) approaches.

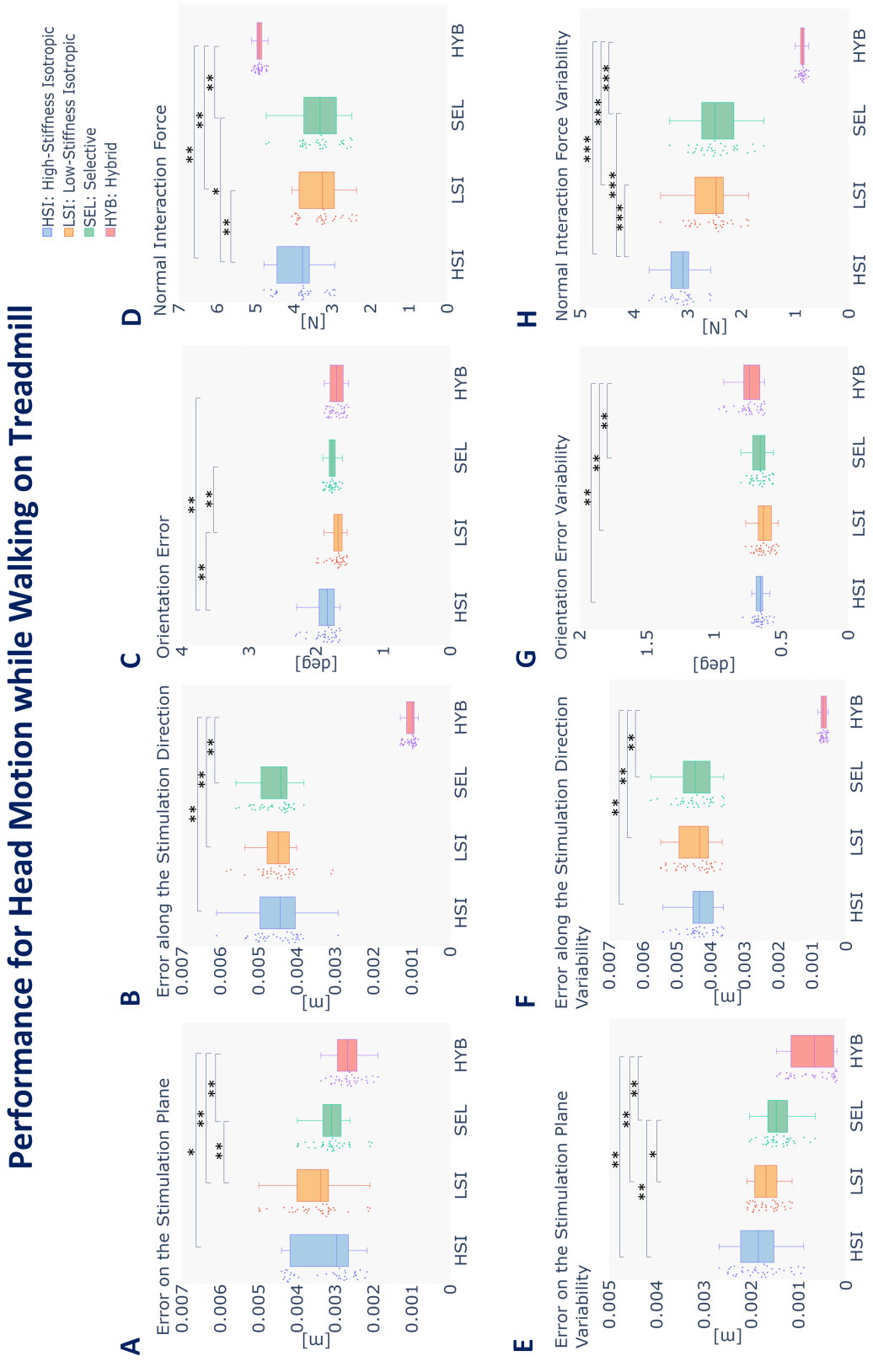

Fig. 3.4 Performance evaluated under dynamic conditions during head motion while walking on a treadmill. Metrics include: A) error on the stimulation plane, B) error along the stimulation direction, C) orientation error, and D) normal interaction force. Panels E–H report the corresponding variability of these metrics. Results are shown for four control strategies: high-stiffness isotropic (HSI), low-stiffness isotropic (LSI), selective impedance (SEL), and hybrid control (HYB). Asterisks indicate a p-value <0.05 (*), <0.01 (**) and <0.001 (***).

Fig. 3.5 Performance evaluated under dynamic conditions for head translations and rotations. Panels A–D report metrics during translational motion: A) error on the stimulation plane, B) error along the stimulation direction, C) orientation error, and D) normal interaction force. Panels E–H show the same metrics during rotational motion. Data are presented for four control strategies: high-stiffness isotropic (HSI), low-stiffness isotropic (LSI), selective impedance (SEL), and hybrid control (HYB). Asterisks indicate a p-value <0.05 (*), <0.01 (**) and <0.001 (***).

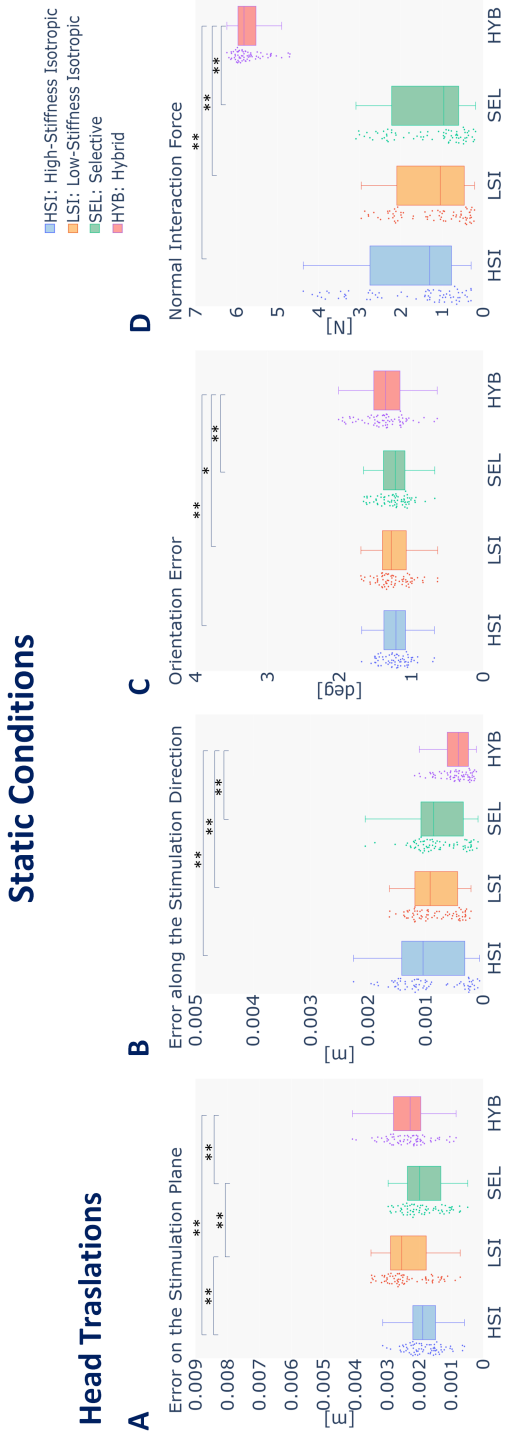

Fig. 3.6 Performance evaluated under dynamic conditions for head translations and rotations. Panels A–D report metrics during translational motion: A) error on the stimulation plane, B) error along the stimulation direction, C) orientation error, and D) normal interaction force. Panels E–H show the same metrics during rotational motion. Data are presented for four control strategies: high-stiffness isotropic (HSI), low-stiffness isotropic (LSI), selective impedance (SEL), and hybrid control (HYB). Asterisks indicate a p-value <0.05 (*), <0.01 (**) and <0.001 (***).

3.2.4 Discussion

We evaluated four control strategies: high-stiffness isotropic impedance, low-stiffness isotropic impedance, selective impedance, and hybrid force-position control under static and dynamic conditions for various head movements. The results show advantages and drawbacks of each approach, providing a clearer understanding of how the potential of TMS can be exploited in new research and clinical applications.

Through the analysis of simulated head movements while walking, our results indicate that, when compared to the other control methods evaluated, the hybrid force-position control achieves the most efficient and stable performance. In particular, the hybrid approach achieves lower errors in the stimulation plane, by ensuring that the coil remains accurately positioned over the target site. The force control along the stimulation axis determines continuous coil-to-scalp contact, which is required for maintaining a consistent and effective stimulation target. Indeed, the induced electric field decays with distance following an inverse-square or inverse-cube law, thus small increases in coil-to-scalp distance cause a significant decrease in the field strength. The hybrid method has significantly less positional and force variability, indicating that it is less prone to perturbations and better able to mantain a stable coil-to-head interaction.

Under dynamic conditions and during continuous translational and rotational head movements, the hybrid force-position strategy again resulted in higher performance. It provided more consistent positioning and lower errors both on the the stimulation and tangential axes compared to impedance-based controls. High-stiffness isotropic impedance strategy provided effective positional accuracy control, but limitations in contact force regulation, resulting in transient force peaks that could adversely affect patient safety and comfort. Low-stiffness isotropic impedance control decreased the force peaks at the cost of a poor accuracy in maintaining the target alignment at the stimulation

site. Selective impedance offered a compromise solution by improving planar accuracy while maintaining moderate pressure on the scalp. Despite these improvements, it performed worse than the hybrid approach in stable coil-to-scalp contact and in accurate alignment during head movements. Thus, the hybrid strategy is particularly adapted for rehabilitation or research protocols where subjects are required to perform an active motor task, as it preserves coil alignment with the stimulation site even during continuous, complex head movements.

In static conditions for both rotational and translational movements, high- stiffness isotropic impedance and selective controls offered greater performance in minimizing coil orientation and stimulation plane errors. Although both approaches showed slightly higher errors along the stimulation axis compared to the hybrid control, those errors remained within acceptable limits [59], [68]. However, since both approaches indirectly manage contact force, they have more variability in force application compared to the hybrid method. This variability can result in occasional pressure fluctuations that can affect patient comfort during extended procedures. Selective control offers a trade-off between the accuracy of coil placement and treatment tolerability. By applying increased stiffness in tangential directions, it reduces planar errors and keeps the coil accurately positioned over the target area. Meanwhile, the lower stiffness along the normal axis prevents excessive scalp pressure and avoids high-force peaks. This targeted stiffness configuration enhances positional accuracy and could improve patient comfort and tolerability for long TMS protocols.

The optimization of the platform has been fundamental in achieving the above results: the integration of low-cost tracking cameras with a higher sampling frequency and the use of open-source neuronavigation software has allowed the development of a platform that has proven to be technical efficient, economically sustainable and potentially accessible even in contexts with limited resources.

The next step will be to assess the system on healthy volunteers and then on clinical populations. This broader experimentation, conducted in real-world scenarios, will help to demonstrate the platform's adaptability and effectiveness, and open up new avenues for innovative clinical and research applications. Feedbacks on patient comfort and system usability will guide further platform refinements.
Moreover, we will integrate virtual and augmented reality systems into the robot-aided TMS platform. This could help the patients immerse themselves in simulated scenarios that replicate real-life situations and implement task-based TMS protocols to potentiate state-dependent plasticity, motor learning and motor adaptation. Further refinements also include the implementation of adaptive closed-loop approaches, in which physiological or neurophysiological signals (e.g., EEG, EMG, HVR) are processed by AI algorithms to adjust the intensity, timing, and target of stimulation in real time, customizing TMS protocols to the patient's needs and potentially increasing their effectiveness.

3.2.5 Conclusion

This study proposes the optimization and the validation of a robotic platform for TMS that offers high precision and adaptability to active patient movement during the procedure.
The platform is composed by a 7-DoF robotic manipulator, a high-frequency optical tracking system, and an open-source neuronavigation software. This configuration provides a versatile, modular, and cost-effective system.
Four different control strategies were implemented and assessed: high-stiffness isotropic impedance, low-stiffness isotropic impedance, selective impedance, and hybrid force-position control. Their performance was evaluated under both static conditions, corresponding to periods when the head was stationary at the end of each simulated movement, and dynamic conditions which involved simulated head motions of increasing complexity, from simple trans-

lational and rotational displacements to more complex motion patterns that replicated walking on a treadmill.

The results defined the strengths and limitations of each approach according to specific operating conditions, accuracy and safety requirements.

The hybrid force-position control strategy most effectively ensure correct coil placemment during active head movements while applying constant and acceptable pressure to the head.

In static stimulation protocols, selective control can be a valid option: this approach reduces planar errors by increasing stiffness in the tangential directions to keep the coil correctly placed over the target area. At the same time, lower stiffness along the normal stimulation axis reduces the pressures exerted on the head.

3.3 Robot-Aided repetitive TMS (rTMS) to Probe Directional Representations in Human Primary Motor Cortex (M1): A Pilot Study

Although the involvement of the primary motor cortex (M1) in the execution of voluntary movements is well-known, it remains unclear which specific aspects of movement are represented, and how they are encoded.
Since the 1980s, a scientific controversy began, and it was centered around two opposing views: one proposing that M1 encodes low-level, effector-specific parameters such as muscle forces or activation patterns (*"M1 knows nothing about movements"*), and the other suggesting that it represents higher-order, extrinsic movement parameters such as trajectory or direction (*"M1 knows nothing about muscles"*) [97].
More recent evidence suggests that a more integrative framework is required, in which M1 activity reflects multiple levels of representation. However, the specific representation of kinematic parameters, such as movement direction, and their contribution to the computation of final motor commands is not yet fully understood.
Recent studies in humans have demonstrated a spatial segregation of movement direction within M1, demonstrating its ability to encode and distinguish the various directions of motion [98], [99], [100]. This raises the question of whether direction-tuned populations in M1 can be selectively modulated. To investigate this, we combined a priming paradigm with state-dependent repetitive TMS (rTMS). In this paradigm, a visual stimulus, indicating the direction of the upcoming movement, transiently pre-activates neuronal populations in M1 that encode a specific movement direction (e.g., vertical or horizontal). With our robot-aided system, rTMS was applied during this brief state of increased excitability, just before movement onset. In this way, stimulation is expected to preferentially modulate the activity of the pre-activated direction-specific population rather than producing a general effect on M1. To assess the

behavioral effects of rTMS, we evaluate changes in motor performance along the primed direction, using measures of trajectory accuracy, smoothness, and movement time.
Thus, we hypothesized that rTMS over M1 selectively modulates motor performance along the primed movement direction compared with sham (vertex) stimulation. We assessed whether motor performance metrics improved relative to baseline during M1 stimulation more than during sham stimulation, and whether these effects persisted after stimulation, for two different movement directions (vertical and horizontal).

3.3.1 Methods

Participants

Fourteen partecipants were recruited in the experiment: 12 females, all right-handed, 24.1± 4.8 aged. All subjects completed a screening questionnaire to identify any possible contraindications to TMS.
The study was approved by the local Ethics Committee (STIMBOY protocol). All participants signed a written informed consent made in accordance with the Declaration of Helsinki and later amendments.

TMS

rTMS was delivered using a Magstim Rapid stimulator (Magstim, UK) connected to a Magstim D70 figure-of-eight coil. Stimulation was triggered by an external TTL input syncronized to the onset of the visual target stimulus. The coil was positioned tangentially over the left primary motor cortex at a site located midway between the cortical representations of the right flexor carpi radialis (FCR) and extensor carpi radialis longus (ECRL) muscles, with an orientation of approximately 45° relative to the midsagittal plane. This intermediate position was selected to allow concurrent but submaximal stimu-

lation of both muscle representations, which lie in close proximity within the primary motor cortex.
MEPs were recorded from both relaxed right muscles using Ag/AgCl surface electrodes placed on each muscle in a belly–tendon montage.
The resting motor threshold (RMT) for each participant, determined at the optimal hotspot for the FCR, was defined as the minimal stimulator output that induced MEPs with peak-to-peak amplitudes ≥ 50 μV in at least 5 out of 10 successive trials. Stimulation intensity during the experimental protocol was set at 80% of RMT [101] and applied at the intermediate coil location to ensure that both FCR and ECRL muscles were effectively activated [102].
During the experimental sessions, the stimulation protocol consisted of short rTMS trains of 3 pulses at 20 Hz (duration $\sim$100 ms) delivered within the $\sim$350 ms reaction window following the target onset.
Depending on the direction of movement to be performed, the stimulation was applied either over the motor hotspot of the left M1, when the target corresponded to the direction under investigation, or over the vertex (active control), when the movement was along the control direction.

Experimental Setup

The experiment was carried out using the robot-aided TMS platform developed by our team, already described in detail in Section 3.2.
The motor task was implemented as a visuomotor game programmed in Unity 3D and integrated into the NeRRoNav neuronavigation [91].
On the screen, four peripheral targets were displayed at 0°, 90°, 180° or 270° along a virtual circumference, with a fifth central target. Cursor position was controlled by a custom 3D-printed wrist-driven manipulandum equipped with reflective markers. The position and orientation of the manipulandum were continuously tracked by the infrared cameras of the neuronavigation system, and a wrist rotation of 20° corresponded to a cursor displacement equal to the

radius of the circumference.
Movements at 0°/180° corresponded to wrist extension/flexion, whereas movements at 90°/270° corresponded to radial/ulnar deviation.
The game was synchronized with the robotic platform through the neuronavigation interface. At the onset of each trial, the system identified the pseudorandom target direction and transmitted the stimulation target to the robot via a UDP communication protocol.
In parallel, the game was also interfaced with a TTL triggering device, which ensured precise timing of rTMS delivery relative to target onset.
As stimulation was programmed to precede movement initiation, the robot continuously adjusted its position during the ongoing trial, so that the coil was correctly aligned with the designated cortical site at the beginning of the subsequent trial. If the subject moved their head slightly immediately before stimulation, the robot compensated for this displacement and the system automatically suspended the trial if the coil positioning error fell below a threshold set by the experimenter (5 mm for position and 5° for orientation) [46], [59].

Experimental Protocol

Participants sat comfortably in front of a computer monitor and used a wrist-driven manipulandum to control the on-screen cursor. The experiment was organised into four blocks, each consisting of 20 trials, with short breaks in between to avoid fatigue (Fig. 3.7 A).
At the start of each trial, the cursor appeared at the central target, corresponding to a neutral wrist position. Then, one of the four peripheral targets was highlighted in red. The order in which the targets were presented within each block was pseudorandomized so that, by the end of a trial, each of the four targets had been presented once.
When a target turned red, participants were asked to perform a centre-out movement, striking the target as quickly and accurately as possible before

returning the cursor to the centre to await the next cue. The maximum time allowed to reach the target was set at 2 seconds.

All participants performed movements in both the horizontal (0°/180°; wrist flexion–extension) and vertical (90°/270°; radial–ulnar deviation) axes (Fig. 3.7 B). Participants were divided into two groups according to the direction in which rTMS was applied over the left M1: one group (n = 7) underwent stimulation during horizontal movements and the other group (n = 7) during vertical movements. For the remaining movement direction, stimulation was applied to the vertex, which was the active control site.

The sequence of sessions was identical for all participants. The first block was carried out without stimulation and served as a baseline; during the second and third blocks, rTMS was applied according to the stimulation protocol described above; the fourth block was performed without stimulation to evaluate whether the effects of rTMS persisted even after stimulation ceased.

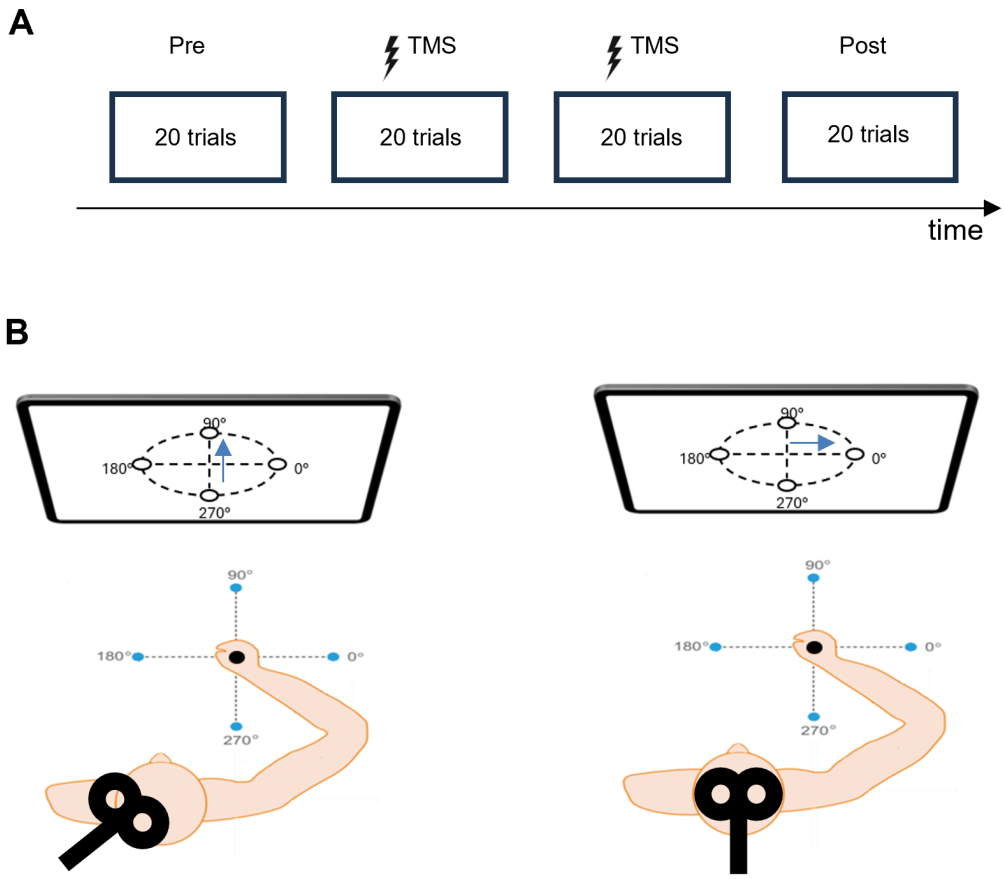

Fig. 3.7 **A:** Session sequence: baseline (no-TMS), two rTMS blocks, and a final no-TMS block to test after-effects. **B:** Participants controlled a screen cursor via a wrist manipulandum and performed center-out wrist movements (flexion–extension; radial–ulnar deviation) toward four targets arranged on a circular layout at 0°, 90°, 180°, and 270°. When the target lay along the task-relevant direction (horizontal in the figure), rTMS was delivered over M1 before movement onset (3 pulses at 20 Hz, 80% RMT). When the movement was along the control direction (vertical in the figure), stimulation was instead applied over the vertex.

3.3.2 Data Analysis

Motor performance of each participant was evaluated using the following parameters:

- Movement time, defined as the time required to reach the target, measured from the appearance of the target;
- Movement smoothness, computed according to the index proposed in [103];
- Absolute directional error, estimated as the area between the actual trajectory followed by the participant and the straight line connecting the center of the screen to the target position.

All parameters were normalized to the baseline condition in order to reduce inter-individual variability and allow a direct comparison of stimulation effects across participants. For each participant, normalization was performed by calculating the relative change from baseline according to the following formula:

$$\frac{x - \text{baseline}}{\text{baseline}}$$

where x represents the mean value of the behavioral metric for each experimental session (stimulation or post-stimulation), computed separately for each stimulation site (M1 or vertex) and for each movement direction (horizontal or vertical), while *baseline* represents the mean value of the same metric in the baseline (no-stimulation) condition for the corresponding stimulation condition and movement direction.
Thus, due to this normalization, motor performance parameters values are dimensionless and reflect proportional changes relative to baseline. For movement time and absolute directional error negative values correspond to improved performance (shorter movement times or smaller errors), while for movement smoothness, positive values correspond to smoother movements.
Statistical analysis was performed using a three-way repeated measures ANOVA, with session (stimulation vs post) and stimulation condition (M1 vs vertex) as within-subject factors, and stimulation direction (horizontal vs vertical) as the between-subject factor.

The normality of data distribution was assessed using the Shapiro–Wilk test; in case of violation of this assumption, the non-parametric Durbin test was employed.
The baseline block (without stimulation) was used exclusively as a reference for data normalization and was not included in the ANOVA.

3.3.3 Results

No significant main effects of session (stimulation vs. post), stimulation condition (M1 vs. vertex) or stimulation direction (horizontal vs. vertical) were detected for any parameters examined (all $p \geq 0.062$).
For movement duration, only a modest trend towards a session effect was observed ($p = 0.062$), but this did not reach significance (See Table 3.2 and Fig. 3.8). The analysis of movement smoothness revealed no significant main effects or interactions, with comparable profiles across conditions (See Table 3.3 and Fig. 3.9). Finally, for directional error, a similar pattern was found, with no reliable effects and only a non-significant tendency towards a session effect ($p = 0.085$) (See Table 3.4 and Fig. 3.10).

Table 3.2 Results of the 3-way ANOVA for normalized movement duration.

Effect	**df**	**F**	**p**
Session	1, 12	4.240	0.062
Stimulation condition (M1 vs. vertex)	1, 12	0.148	0.707
Stimulation direction (horizontal vs. vertical)	1, 12	0.423	0.527
Session × Stimulation condition	1, 12	0.077	0.787
Session × Stimulation direction	1, 12	0.112	0.743
Stimulation condition × Stimulation direction	1, 12	1.105	0.314
Session × Stimulation condition × Stimulation direction	1, 12	1.553	0.237

Note. Type III sums of squares were used.

Table 3.3 Results of the 3-way ANOVA for normalized movement smoothness.

Effect	**df**	**F**	**p**
Session	1, 12	0.226	0.643
Stimulation condition (M1 vs. vertex)	1, 12	0.739	0.407
Stimulation direction (horizontal vs. vertical)	1, 12	0.005	0.943
Session × Stimulation condition	1, 12	1.034	0.329
Session × Stimulation direction	1, 12	0.208	0.656
Stimulation condition × Stimulation direction	1, 12	0.716	0.414
Session × Stimulation condition × Stimulation direction	1, 12	0.282	0.605

Note. Type III sums of squares were used.

Table 3.4 Results of the 3-way ANOVA for normalized directional error.

Effect	**df**	**F**	**p**
Session	1, 12	3.533	0.085
Stimulation condition (M1 vs. vertex)	1, 12	0.006	0.939
Stimulation direction (horizontal vs. vertical)	1, 12	0.192	0.669
Session × Stimulation condition	1, 12	1.824	0.202
Session × Stimulation direction	1, 12	0.797	0.389
Stimulation condition × Stimulation direction	1, 12	1.206	0.294
Session × Stimulation condition × Stimulation direction	1, 12	0.055	0.819

Note. Type III sums of squares were used.

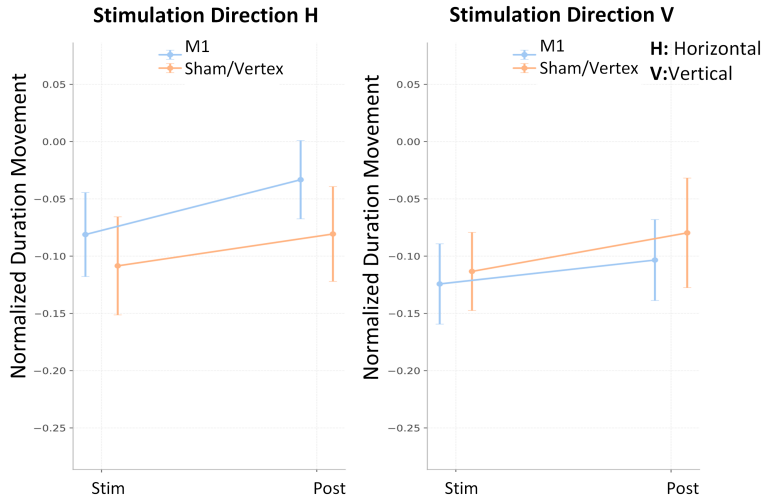

Fig. 3.8 Normalized movement duration for horizontal (H) and vertical (V) stimulation directions. Data are shown for the stimulation (Stim) and post-stimulation (Post) sessions in both experimental conditions: M1 and Sham/Vertex. Normalized values are expressed as relative, dimensionless changes from baseline.

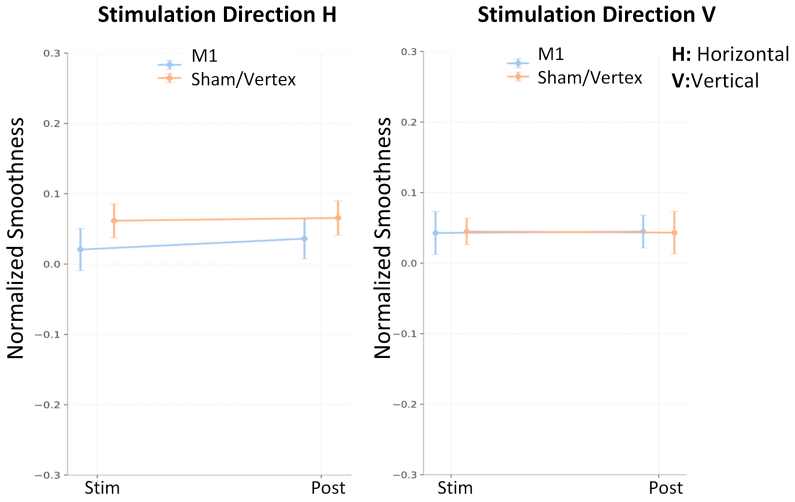

Fig. 3.9 Normalized smoothness for horizontal (H) and vertical (V) stimulation directions. Data are shown for the stimulation (Stim) and post-stimulation (Post) sessions in both experimental conditions: M1 and Sham/Vertex. Normalized values are expressed as relative, dimensionless changes from baseline.

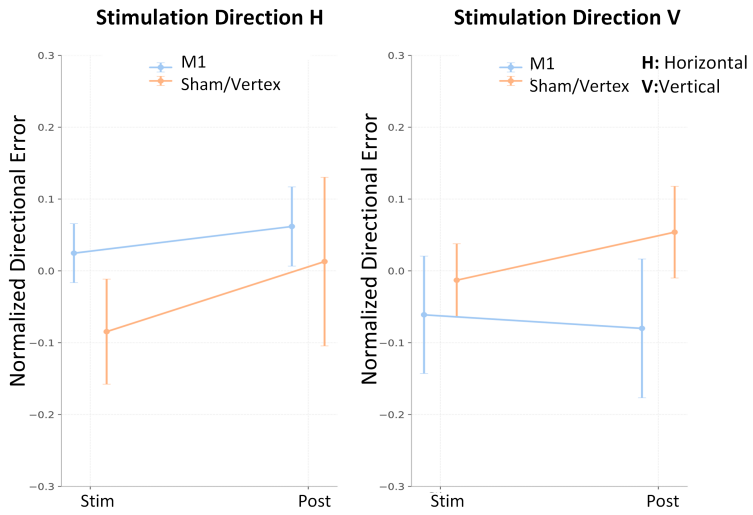

Fig. 3.10 Normalized directional error for horizontal (H) and vertical (V) stimulation directions. Data are shown for the stimulation (Stim) and post-stimulation (Post) sessions in both experimental conditions: M1 and Sham/Vertex. Normalized values are expressed as relative, dimensionless changes from baseline.

3.3.4 Discussion

The idea behind this study was ambitious: to test whether it was possible to selectively modulate directionally tuned neuronal populations in M1 by combining rTMS and a priming paradigm. We combined a visual directional prime with short trains of high-frequency rTMS, delivered during movement preparation, with the aim of modulating the activity of pre-activated populations coding for a specific movement direction.

The rationale was grounded on neurophysiological and neuroimaging evidence attesting to the existence of segregated directional representations in M1 [98], as well as on the principle of state-dependent TMS, according to which stimulation is more selective and effective when applied to neuronal populations that are already partially active [104].

However, the results of our study did not confirm the hypothesis of a systematic behavioural effect resulting from the interaction between priming and

rTMS. Measures of movement time, smoothness and directional accuracy revealed no significant differences between conditions, directions or sessions. Here, we analyze several plausible causes of these null results in more detail. In a state-dependent paradigm, the precise timing of rTMS stimulation relative to the desired cortical state is a major factor influencing its effectiveness. In our protocol, the rTMS trains were synchronized with the appearance of the visual target. However, it is possible that the window of maximum neuronal excitability varied from person to person and from trial to trial, making precise alignment difficult. The literature shows that during movement preparation the excitability of M1 is modified in a task- and muscle-specific manner, reflecting the anticipatory specification of the forthcoming movement [105]. Therefore, the fluctuating dynamics of the preparatory state can profoundly influence the effects of stimulation. Thus, without an online cortical state monitoring system, the sensitivity of our protocol may have been significantly reduced.

Moreover, the stimulation parameters were very conservative, involving relatively low-intensity stimulation (80% of the individual RMT) delivered in short trains ($\sim$100 ms) of only three pulses. While this configuration was safe and well-tolerated by participants, it is possible that the stimulation was too weak or brief to produce measurable behavioural effects [106].

Another limitation could be the nature of the motor task. Participants performed highly consolidated and automated movements (wrist flexion-extension and deviation), which could involve distributed, robust, and redundant circuits. In such cases, even selective disruption of M1 could be compensated for by other cortical or subcortical regions, maintaining motor performance unchanged.

Furthermore, in future experiments, it may be important to control for inherent motor learning occurring already during the baseline phase and throughout the protocol, for example by stabilizing performance prior to stimulation, to ensure that performance improvements can be attributed to rTMS rather than

to practice effects.

However, despite the lack of results, our study presents a highly relevant methodological aspect: the use of a robotic platform for innovative TMS protocols. This system ensured higher stability in coil positioning and enabled trial-by-trial dynamic realignment according to the specific experimental condition. Thanks to synchronization between the visuomotor task, the neuronavigation system and the robotic arm, the coil was automatically repositioned on the M1 cortical site corresponding to the stimulation direction, or on the vertex in control conditions. This ensured that each individual trial was precisely associated with the correct stimulation site. Such rapid and accurate realignment would not have been possible manually.

3.3.5 Conclusion

Although this experiment did not lead significant results, it nevertheless highlights the practical challenges of attempting to selectively modulate specific neuronal populations in M1. These findings should be viewed as a valuable opportunity to refine the proposed stimulation protocol and to consider the integration of complementary methodological approaches, in order to better understand the complex functional organization of the motor cortex.

Future studies should aim to improve temporal precision, possibly through online monitoring of cortical states, and to explore stimulation parameters better suited to induce measurable effects. In parallel, employing less automatized motor tasks may enhance sensitivity to M1 perturbation.

3.4 Robot-Aided EEG-Informed TMS: Phase-Specific Modulation of the Mu Rhythm

Although the introduction of robot-aided TMS platforms can reduce spatial sources of variability by improving accuracy, repeatability, and reliability of clinical and research TMS protocols [34], [60], [61], the heterogeneity of TMS results continues to be partially influenced by the brain ongoing functional state at the time of stimulation [104].
Conventionally, TMS is delivered in a standardized manner: the brain is treated as a static system and stimulated according to a predefined protocol. This approach ignores the concept of state-dependency, which proposes that the effectiveness of stimulation is also influenced by the neurophysiological state of the brain at the time of the TMS intervention [104], [107].

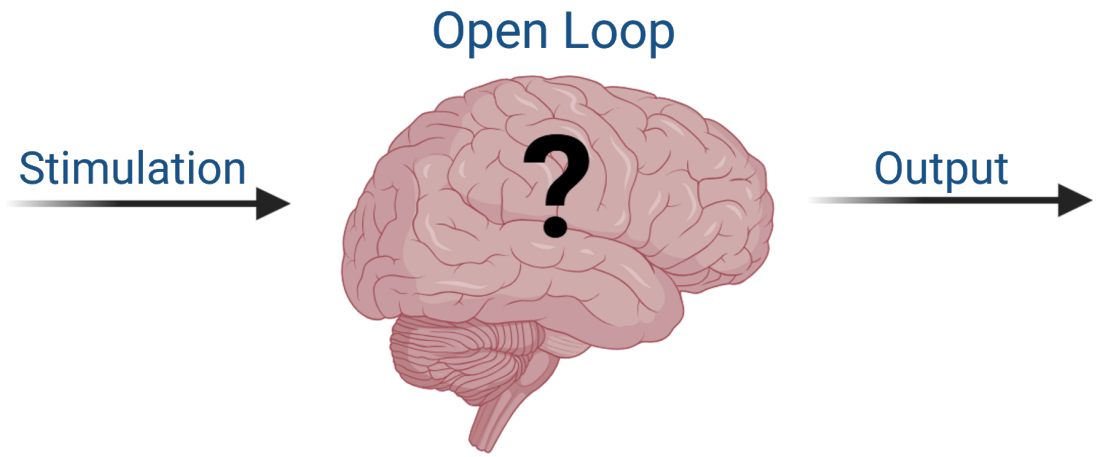

Fig. 3.11 Schematic representation of the conventional open-loop TMS approach: stimulation is delivered according to predefined parameters without accounting for the ongoing neurophysiological state of the brain.

TMS can be combined with electroencephalography (EEG) and a robotic platform to obtain a setup that is able to control both the timing and location of stimulation with high accuracy. Specifically, EEG allows continuous real-time monitoring of oscillatory neuronal activity to synchronize TMS pulses with specific ongoing brain events. Meanwhile, the robotic system ensures high spatial accuracy of coil placement, by maintaining it fixed at the stimulation site even during involuntary subject head movements. Due to the limited widespread of robot-aided TMS platforms, the majority of EEG-informed TMS studies have been conducted without robotic assistance and stimulation is typically delivered manually, with spatial accuracy depending on the operator's expertise.

Most of this work has focused on synchronizing TMS stimulus delivery with specific phases of the sensorimotor mu rhythm to assess the effects on corticospinal excitability as reflected in the amplitude of motor evoked potentials (MEPs) [31], [108].

Phase prediction algorithms typically fall into two main categories: signal prediction and single-point prediction [109]. The first approach predicts the entire signal over a future time window and allows the phase to be calculated at any point within that interval. One of the first successful application was the implementation of an algorithm where an autoregressive model was used to predict the entire future signal, and the target phase was then determined using the Hilbert transform [110], [111]. On the other hand, the second approach directly estimates the precise moment at which a given phase occurs without reconstructing the entire signal. Studies in this context have proposed solutions based on the analysis of the distance between successive peaks [112], [113], [114] or the use of Fourier [115] or wavelet transforms [116] to derive the instantaneous target phase.

However, in both types of approach, the final portion of the signal window is not reliably used for real-time applications. Indeed, most of them involve the use of digital filters that introduce distortions at the edges of the signal due to

incompleteness of the data window. Similarly, methods using mathematical transforms are less accurate in phase estimation near temporal boundaries, where the information symmetry is lost due to the absence of future samples. These structural limitations necessarily require the implementation of a signal prediction strategy to compensate for the lack of reliably phase estimates in the immediate present and to try to achieve a good level of accuracy in the synchronization between stimulation and brain oscillatory state.
Therefore, we introduce a novel real-time brain state-EEG informed-TMS approach which does not require filters or transformations and can directly exploit the most recent data within the sliding window to enable an accurate real-time phase detection. This approach is combined with a robot-aided TMS platform which offers high spatial accuracy and repeatability, keeping the coil positioned over the stimulation target throughout the experimental session, even in presence of subject head movements. We targeted the mu rhythm at its peak and trough, as well as the phases of the intermediate point of the ascending phase (from trough to peak), and the intermediate point of the descending phase (from peak to trough) to assess if stimulation delivered at these distinct phases may modulate corticospinal excitability.

3.4.1 Methods

Participants

Six right-handed female participants, aged 23 ± 2, were recruited for the experiment. All subjects completed a screening questionnaire to identify any possible contraindications to TMS. Selection criteria did not include specific TMS-related parameters, such as resting motor threshold, nor EEG-related features, such as the presence of a well-defined peak of the mu rhythm power spectrum.
This study was conducted after approval of the local Ethics Committee of

University of Regensburg (protocol number: 25-4130-101), in accordance with the Declaration of Helsinki and following amendments.

TMS

Single-pulse TMS was administered using a Cool-B35 figure-of-eight coil connected to a MagVenture X100 stimulator (MagVenture A/S, Denmark). Stimuli were activated by an external TTL trigger input from the real-time EEG system.

The coil was positioned over the left primary motor cortex, at the location that corresponds to the cortical representation of the right first dorsal interosseous (FDI) muscle, oriented at approximately 45° relative to the midsagittal plane. MEPs were collected from the relaxed right FDI through disposable self-adhesive surface electrodes arranged in a belly–tendon configuration.

Coil positioning and orientation were continuously tracked by stereotactic neuronavigation (Localite GmbH, Sankt Augustin, Germany) and maintained on the stimulation hotspot throughout the experiment by a robotic arm (Cobot, Axilium Robotics, France), which provides stable coil placement. If the subject slightly moved the head immediately before stimulation, the robotic system compensated for the displacement. The trial was automatically paused whenever the coil placement error exceeded a threshold defined by the operator: 5 mm for position and 5° for orientation [59].

The motor hotspot was defined as the scalp location where a TMS pulse evoked MEPs of maximal amplitude in the contralateral FDI muscle. The resting motor threshold (RMT) was subsequently determined at this site as the minimal stimulator output intensity that produces MEPs with a peak-to-peak amplitude of ≥ 50 μV in at least 5 out of 10 consecutive stimulations. The stimulation intensity for the experimental sessions was set to 110% of the individual RMT.

EEG recordings

EEG was recorded using a TMS-compatible 64-channel actiCHamp Plus amplifier (Brain Products GmbH, Germany) at a sampling rate of 10 kHz. Recordings were obtained from 62 passive Ag/AgCl electrodes integrated into a TMS-compatible EEG cap, using the standard 10–20 configuration [117]. Ground and reference electrodes were positioned symmetrically on the partecipant's forehead, with the ground on the left and the reference on the right.
To maintain good signal quality, an electroconductive abrasive gel was applied to keep electrode impedance lower than 5 kΩ, with regular checks performed before and during the experimental session.
To enable real-time EEG stimulation, the TMS-compatible amplifier was connected to the TurboLink module (Brain Products GmbH), which provided ultra-low latency digital streaming (< 1.5 ms) via UDP. TurboLink was configured to continuously stream a user-defined subset of EEG channels (See next paragraph for more details) to a client PC that performed online signal processing routines for stimulation control. In parallel, raw EEG data were stored on a dedicated recording PC for offline analysis.

EEG Signal Processing and Algorithm Architecture

The EEG-informed TMS algorithm was developed in Python 3.11 and it is divided into two stages: an offline phase, dedicated to the extraction of an individualized mu rhythm oscillatory template, and an online phase, during which real-time stimulation is delivered based on the ongoing mu activity.
During the offline phase, resting-state EEG recording was processed through a custom analysis pipeline.
To reduce the effects of volume conduction and minimize contributions from non-motor alpha sources, a Hjort trasnformation was applied. The resulting Hjorth-C3 signal, computed from electrode C3 and its eight nearest neighbors

(FC1, FC3, FC5, C5, CP5, CP3, CP1, C1), was then used to estimate each participant's mu rhythm template.

The Power Spectral Density (PSD) of the Hjorth-C3 signal was analyzed to identify the dominant mu peak frequency and to define an individualized mu band, within which the signal was band-pass filtered using a second-order Butterworth filter.

Mu rhythm activity was detected based on its negative peaks, which provide a more stable and consistent phase-locking marker than positive deflections, due to their higher amplitude and sharper morphology.

To consider the variability in amplitude of mu activity across participants, a subject-specific threshold was applied to select only negative peaks with a higher signal-to-noise ratio (SNR). Thus, the threshold was calculated based on the distribution of negative peaks recorded during the resting-state EEG, such that amplitudes exceeding two standard deviations from the mean were classified as mu activity.

Epochs of 400 ms centered on each detected trough were extracted and subsequently averaged to generate a subject-specific mu-rhythm template waveform.

From this subject-specific mu waveform, four phase-specific templates were derived. Each template represented the same oscillatory cycle but was phase-shifted to align with one of four characteristic points: the negative peak, mid-ascending phase, positive peak, and mid-descending phase.

These templates were then used as reference models for the subsequent online stimulation phase. During the online stimulation phase, EEG data were continuously acquired and processed in real time.

For each trial, one of the four target phases was randomly assigned according to a randomized block design. The real-time Hjorth-C3 signal was continuously correlated with the precomputed template associated with that specific target phase. Specifically, the system performed a correlation between the most recent EEG segment and the selected phase template (Fig. 3.12). When

the correlation coefficient exceeded a threshold of r=0.85, the ongoing signal was found to match the desired phase pattern. At that moment, a phase-consistent event was detected and a TMS pulse was automatically triggered via an external TTL signal.

The algorithm imposed a minimum ISI of 2 seconds to prevent phase-resetting effects.

System latency, measured from EEG acquisition to TTL pulse delivery, remained below 5 ms.

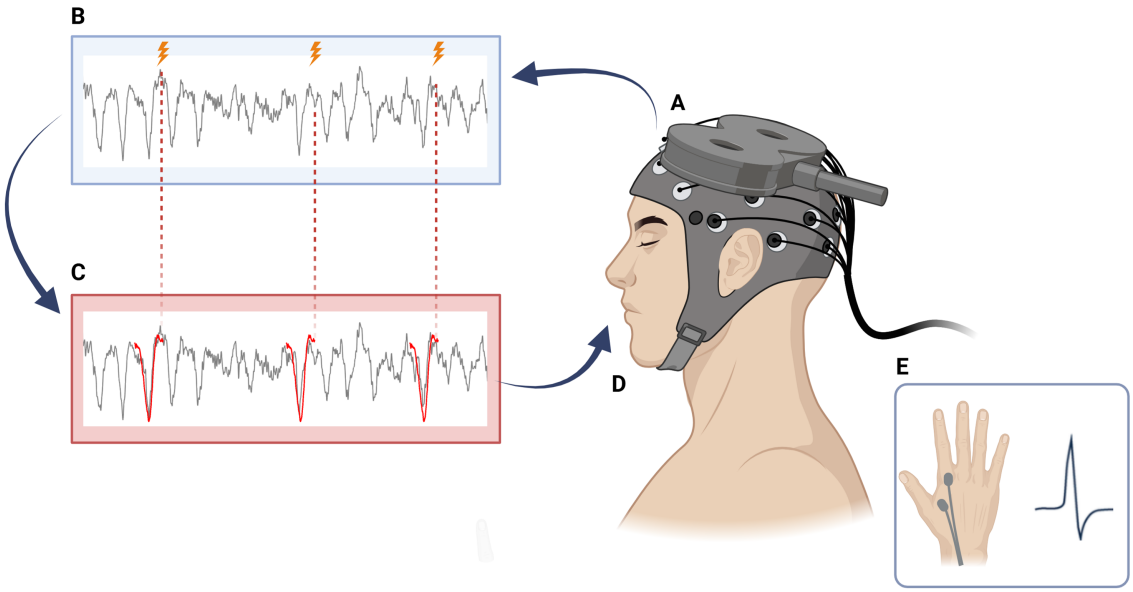

Fig. 3.12 Schematic representation of the EEG-informed TMS algorithm. **(A)** A participant wearing an EEG cap with a TMS coil positioned over the left motor cortex. **(B)** Real-time EEG monitoring of the Hjorth-C3 signal reveals ongoing mu rhythm oscillations. **(C)** Target phase detection within the individualized mu band, based on correlation with precomputed templates. **(D)** When a matching phase pattern is detected, a TMS pulse is delivered. **(E)** Motor-evoked potentials (MEPs) are recorded from the contralateral FDI muscle.

Experimental protocol

Throughout the experiment, participants were seated comfortably and asked to stay relaxed, maintaining a resting state with eyes open during the recordings. Within this setting, the experimental protocol consisted of three consecutive

phases.
In the preparatory phase, the EEG cap was mounted, the motor hotspot was identified, and the resting motor threshold was determined.
Participants then completed a five-minute resting EEG recording with eyes open while fixating a cross located one metre away.
Subsequently, participants received single-pulse TMS delivered at four distinct phases of the Hjorth-C3 signal: the positive peak, the negative peak, the intermediate point of the ascending phase (from trough to peak), and the intermediate point of the descending phase (from peak to trough).
Within each block of 40 trials, 10 stimuli were delivered for each condition. This block was repeated three times, separated by 1–2 min rest intervals, resulting in a total of 120 stimuli.
The order of conditions within each block was randomized.
Each experimental session, including setup and all stimulation phases, lasted approximately three hours.

3.4.2 Data Analysis

EMG Processing

Offline analysis of EMG data was conducted using Matlab (The MathWorks, Inc., Natick, MA). MEP peak-to-peak amplitudes were computed as the difference between the highest and lowest voltage values occurring within 20–40 ms after each TMS pulse.
Trials with pre-activation of the target muscle in the pre-stimulus window (-100 to 0 ms) were visually identified and excluded from following analysis.

Statistical Analysis

To assess the effect of the target phase on corticospinal excitability, we employed a Linear Mixed-Effects Model.

The amplitude of the MEPs, the dependent variable, was log-transformed before analysis to satisfy the residuals' normality assumptions.
The model included Phase Condition as a fixed effect with four levels corresponding to the target phases of the mu rhythm (Negative Peak, Ascending Phase, Positive Peak, Descending Phase), and a random intercept for Subject to consider the inter-individual variability and the inherently hierarchical nature of the repeated-measures data.
In the case of a significant main effect, pairwise post-hoc comparisons between all levels of the experimental condition were employed to identify the specific differences.

3.4.3 Results

Despite the inter-individual variability in MEP amplitudes (Fig. 3.13), a clear and consistent phase-dependent pattern emerged. Larger responses were typically elicited around the negative peak and the rising slope of the mu oscillation, whereas smaller MEPs occurred near the positive peak and falling slope. The employed Linear Mixed Model showed a significant main effect of Phase Condition ($F(3, 716) = 17.14$, $p < 0.001$).
Post-hoc pairwise comparisons revealed that MEP amplitudes were significantly higher during the negative peak and rising slope compared to both the positive peak and falling slope (all $p < 0.001$). Additionally, no significant difference was found between the negative peak and rising slope ($p = 0.18$), nor between the positive peak and falling slope ($p = 0.10$) (Fig. 3.14).

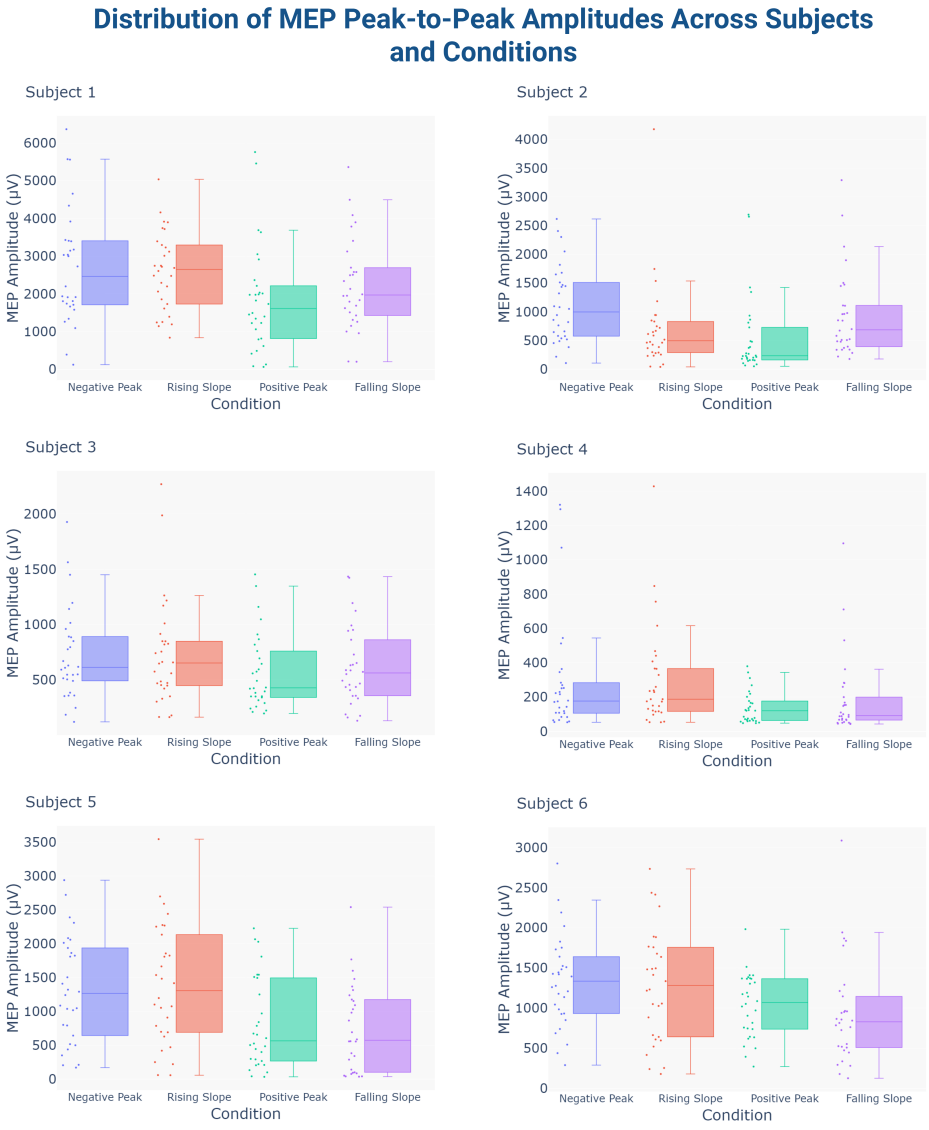

Fig. 3.13 Distribution of MEP peak-to-peak amplitudes across subjects and conditions. Each boxplot represents the distribution of MEP amplitudes (in μV) measured at four points of the oscillatory phase of the mu signal (Negative Peak, Rising Slope, Positive Peak, Falling Slope). Data are shown separately for each subject (from 1 to 6).

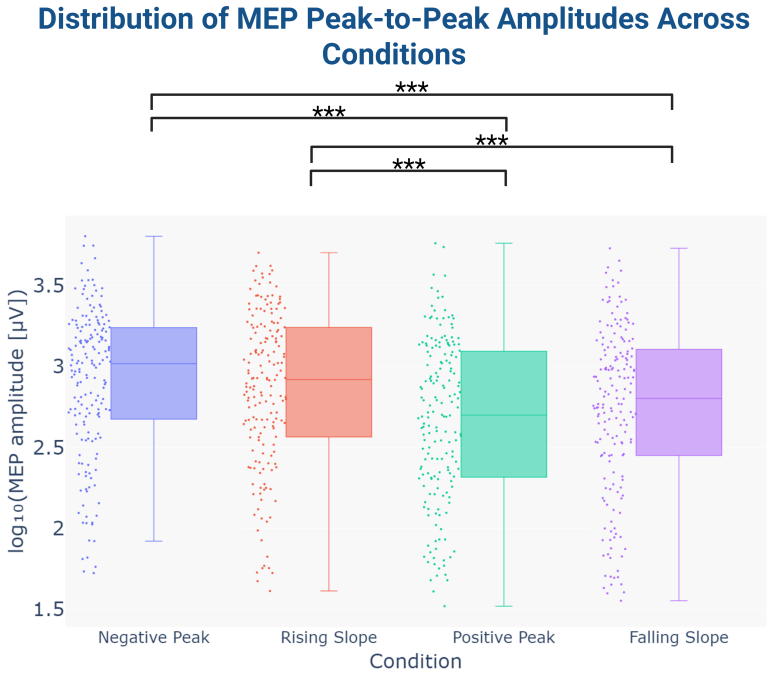

Fig. 3.14 Distribution of MEP peak-to-peak amplitudes across experimental conditions. Boxplots illustrate the distribution of log10 transformed MEP peak-to-peak amplitudes (in μV) for each oscillatory phase condition (Negative Peak, Rising Slope, Positive Peak, and Falling Slope). Dots represent individual data points pooled across subjects. Significant differences between conditions are indicated by asterisks (*** $p < 0.001$).

3.4.4 Discussion

This study introduces a new phase targeting algorithm developed to overcome the structural limitations of existing approaches. Traditional methods, based on digital filtering techniques [110], [111], [113] or mathematical transformations [115], [116] are often affected by artifacts at the temporal edges of the signal. Since the final portion of the signal is unreliable, these approaches do not have a most recent reference point and must therefore resort to predictive models to estimate when the target phase will occur. In contrast, the proposed algorithm operates in real time and exploits only the most recent EEG data, which is continuously compared with a mu rhythm template specific to each

participant. In contrast, the proposed algorithm operates in real time and exploits only the most recent EEG data, which is continuously compared with a mu rhythm template specific to each participant. Furthermore, unlike approaches that excessively manipulate the signal and can lead to an estimate of the target phase that is far from the actual intrinsic neural dynamics, our method preserves the individual morphology of the mu rhythm, allowing TMS to be synchronized with a well-defined, specific and reproducible neurophysiological state.

Using this algorithm, we investigated how corticospinal excitability varies as a function of the instantaneous phase of the mu rhythm when TMS is delivered in synchrony with ongoing brain activity.

The results showed a phase-dependent modulation of corticospinal excitability: MEP amplitudes were greater when stimulation occurred near the negative peak and during the ascending phase of the mu rhythm, while they were significantly suppressed near the positive peak and in the descending phase [111], [118].

Higher excitability around the negative peak may reflect a transient increase in the depolarization of pyramidal neurons that promotes synchronization and facilitates TMS-induced cortical recruitment. In contrast, the reduction in MEP amplitudes around the positive peak may indicate hyperpolarization or an increase in local inhibitory mechanisms that limit the likelihood of a response. These results support the view that the mu rhythm might function as a dynamic gating mechanism within sensorimotor circuits, modulating cortical excitability through alternations between excitatory and inhibitory network states [111]. In future studies, however, it would be useful to combine phase-specific conditions with stimulation that is not phase-locked to the mu rhythm, in order to allow a direct comparison with traditional TMS. This would help to better understand whether the observed effects truly depend on stimulation timing and whether phase targeting affects the variability of responses across subjects.

Overall, the results suggest that the temporal dimension is an important factor in non-invasive brain stimulation. The brain's response to external input does not depend solely on the intensity or location of the stimulation, but also on the neurophysiological functional state at the time of intervention. Thus, temporal synchronization between TMS stimulation and the optimal phase of the endogenous oscillatory activity may improve the effectiveness of treatment, but also the reliability and the predictability of the neurophysiological effects of TMS, while potentially reducing the inter-individual variability that traditionally limits the robustness of experimental and clinical results.

3.4.5 Conclusion

In conclusion, this study introduces a new real-time EEG-informed TMS algorithm capable of identifying specific phases of mu oscillatory activity without relying on predictive models.
The results show that corticospinal excitability may be dynamically modulated by the instantaneous phase of the sensorimotor mu rhythm. In particular, TMS pulses delivered around the negative peak and during the ascending phase of the mu oscillation generated significantly larger MEPs than those delivered at the positive peak and in the descending phase.
However, in future we should verify whether the proposed approach can be generalized to other frequency bands and/or implemented in rTMS protocols, evaluating its application to the clinical population as well.

Chapter 4

Conclusion and Future Outlook

Although TMS is a relatively new technique, with only four decades of history, it has already become a consolidated and versatile tool for a wide range of applications, from research to clinical purposes [3], [119]. However, the variability of its results still limits its full potential. This inconsistency arises from the complexity of managing multiple sources of variability: on one hand, extrinsic factors related to the subjects, including, for instance, brain anatomy and brain activity state during the stimulation session [120], [121], [122]; on the other hand, intrinsic factors related to the technique itself, such as coil positioning accuracy and stimulation [8], [33], [123].

Recent scientific and technological landscape offers promising opportunities: the latest advances, from the introduction of robot-aided TMS platforms that ensure high spatial accuracy, to the development of intelligent algorithms that process neurophysiological signals and customize the stimulation, constitute a concrete step toward the development of more reliable and effective stimulation protocols [120], [123], [124].

In this still emerging scenario, this thesis ultimately aimed to investigate how the use of a robot-aided TMS platform could foster the implementation of more precise, flexible, and tailored stimulation paradigms that would be too challenging for a human operator.

The starting point was the optimization and validation of a robot-aided TMS platform to achieve a modular, flexible, and economically sustainable system. By implementing and validating different control strategies, the platform was tested in static and dynamic conditions. In particular, in the latter conditions, which represent an innovative use of TMS, the system proved to be a powerful methodological tool for the implementation of new stimulation paradigms that can be administered during the execution of complex motor tasks, such as walking. This approach opens up interesting prospects for a more detailed understanding of motor control and motor learning mechanisms, and for their use in more targeted rehabilitation treatments for movement disorders.

The next step was to employ this methodology in complex and advanced stimulation protocols. Exploiting the spatial accuracy and dynamicity of robot-aided TMS platforms, this work investigated a further dimension: that of state-dependency. A robot-aided rTMS protocol, combined with a directional priming paradigm, was proposed to investigate the possibility of selectively probing populations of neurons that encode a specific direction of movement during the preparatory phase of the action. Although the behavioral results were inconclusive, probably due to a combination of factors, including the absence of cortical activity monitoring to determine the optimal timing for rTMS delivery and the limited sensitivity of the behavioral task performed, the use of robot-aided TMS platform in this experimental design was fundamental. It allowed for rapid and accurate repositioning between distinct cortical sites (M1 and vertex), trial by trial and according to the specific experimental condition, with a time interval of less than two seconds.

Finally, this work achieved a qualitative leap by integrating the spatial accuracy provided by the robot-aided TMS platform with the temporal precision of EEG. An EEG-informed TMS approach was developed, enabling real-time synchronization of TMS delivery with specific phases of each participant's endogenous mu rhythm. The results were promising, confirming that corti-

cospinal excitability is not constant but fluctuates, being higher during the descending phase and at the negative peak of the mu rhythm, and reduced at the positive peak. The brain's response to external input does not depend solely on the intensity or location of the stimulation, but also on the neurophysiological functional state at the time of intervention, the temporal synchronization between TMS stimulation and the ongoing brain activity could amplify the effectiveness of treatments, but also the reliability and the predictability of the neurophysiological effects of TMS.

These achievements, however, should not be seen as the end of a journey, but as the groundwork for an even more ambitious research program.
The most immediate direction is a rigorous and gradual clinical validation process, aimed at translating the technical advantages of the robot-aided TMS platform into tangible benefits for patients, accompanied by continuous technical refinement of the system to improve its robustness, usability, and accessibility. At the same time, the solid foundations laid by the EEG-informed TMS approach need to be explored to their full potential, generalizing its use to other frequency bands (e.g, beta, gamma) and implementing it in rTMS protocols to verify its ability to induce more robust and lasting plasticity.
The ultimate goal, which combines all these threads, is the realization of an integrated, closed-loop stimulation platform. This system would combine robotics with artificial intelligence algorithms capable of automatically adapting not only the position of the coil, but also the intensity and timing of the stimulation based on the patient's neurophysiological signals. Further synergy with Virtual and Augmented Reality technologies would complete this architecture, creating more immersive and engaging stimulation environments and allowing their application in more dynamic and functionally significant settings.

References

[1] Juliana Basulo-Ribeiro and Leonor Teixeira. The future of healthcare with industry 5.0: preliminary interview-based qualitative analysis. *Future Internet*, 16(3):68, 2024.

[2] LA Geddes. History of magnetic stimulation of the nervous system. *Journal of Clinical Neurophysiology*, 8(1):3–9, 1991.

[3] A. T. Barker, R. Jalinous, and I. L Freeston. Non-invasive magnetic stimulation of human motor cortex. *Lancet*, 1(8437):1106–1107, 1985.

[4] Mark Hallett. Transcranial magnetic stimulation: a primer. *Neuron*, 55(2):187–199, 2007.

[5] Steffen Angstmann and Hartwig Roman Siebner. Effects of cortical stimulation on cortical functional connectivity: Imaging studies. In *Cortical Connectivity: Brain Stimulation for Assessing and Modulating Cortical Connectivity and Function*, pages 71–91. Springer, 2012.

[6] Fahad A Somaa, Tom A de Graaf, and Alexander T Sack. Transcranial magnetic stimulation in the treatment of neurological diseases. *Frontiers in neurology*, 13:793253, 2022.

[7] Ali Yadollahpour, Samaneh Rashidi, and Pramod Singh Kunwar. Repetitive transcranial magnetic stimulation in psychiatric disorders: a review of clinical advances. *Asian J Pharm*, 11(2):S242–50, 2017.

[8] Nikolai H Jung, Igor Delvendahl, Nicola G Kuhnke, Dieter Hauschke, Sabine Stolle, and Volker Mall. Navigated transcranial magnetic stimulation does not decrease the variability of motor-evoked potentials. *Brain stimulation*, 3(2):87–94, 2010.

[9] Cecilia Nauczyciel, Pierre Hellier, Xavier Morandi, Sophie Blestel, Dominique Drapier, Jean Christophe Ferre, Christian Barillot, and Bruno Millet. Assessment of standard coil positioning in transcranial magnetic stimulation in depression. *Psychiatry research*, 186(2-3):232–238, 2011.

[10] Eric M Wassermann, C Epstein, U Ziemann, V Walsh, T Paus, and S Lisanby. Inter-and intra-individual variation in the response to tms. In *Oxford Handbook of Transcranial Stimulation*, page 401. Oxford University Press, 2008.

[11] Davide B Cappon and Alvaro Pascual-Leone. Toward precision noninvasive brain stimulation. *American Journal of Psychiatry*, 181(9):795–805, 2024.

[12] Roland Sparing, Maike D Hesse, and Gereon R Fink. Neuronavigation for transcranial magnetic stimulation (tms): where we are and where we are going. *Cortex; a journal devoted to the study of the nervous system and behavior*, 46(1):118–120, 2010.

[13] Isabella M Young, Karol Osipowicz, Alana Mackenzie, Oliver Clarke, Hugh Taylor, Peter Nicholas, Mark Ryan, Jonas Holle, Onur Tanglay, Stephane Doyen, et al. Comparison of consistency between image guided and craniometric transcranial magnetic stimulation coil placement. *Brain Stimulation: Basic, Translational, and Clinical Research in Neuromodulation*, 15(6):1465–1466, 2022.

[14] URL: https://psychscenehub.com/psychinsights/transcranial-magnetic-stimulation-for-depression/.

[15] Muhannad M Alsharidah, Mohammad Uzair, Sarah S Alseneidi, Afnan A Alkharan, Reem Fahd Bunyan, and Shahid Bashir. The role of transcranial magnetic stimulation as a surrogate marker of disease activity in patients with multiple sclerosis: a literature review. *Innovations in Clinical Neuroscience*, 19(1-3):8, 2022.

[16] Marion Simpson and Richard Macdonell. The use of transcranial magnetic stimulation in diagnosis, prognostication and treatment evaluation in multiple sclerosis. *Multiple sclerosis and related disorders*, 4(5):430–436, 2015.

[17] A Nascimbeni, A Gaffuri, L Granella, M Colli, and P Imazio. Prognostic value of motor evoked potentials in stroke motor outcome. *European Journal of Physical and Rehabilitation Medicine*, 41(2):125, 2005.

[18] Ana Dionisio, Isabel Catarina Duarte, Miguel Patricio, and Miguel Castelo-Branco. The use of repetitive transcranial magnetic stimulation for stroke rehabilitation: a systematic review. *Journal of stroke and cerebrovascular diseases*, 27(1):1–31, 2018.

[19] Jodi D Edwards, Adan Ulises Dominguez-Vargas, Charlotte Rosso, Meret Branscheidt, Lisa Sheehy, Fanny Quandt, Simon A Zamora, Melanie K Fleming, Valentina Azzollini, Ronan A Mooney, et al. A translational roadmap for transcranial magnetic and direct current stimulation in stroke rehabilitation: Consensus-based core recommendations from the third stroke recovery and rehabilitation roundtable. *International Journal of Stroke*, 19(2):145–157, 2024.

[20] Basavana Goudra, Dipal Shah, Ganesh Balu, Gowri Gouda, Alan Balu, Anuradha Borle, and Preet Mohinder Singh. Repetitive transcranial magnetic stimulation in chronic pain: a meta-analysis. *Anesthesia Essays and Researches*, 11(3):751–757, 2017.

[21] Shawn Zardouz, Lei Shi, and Albert Leung. A feasible repetitive transcranial magnetic stimulation clinical protocol in migraine prevention. *SAGE open medical case reports*, 4:2050313X16675257, 2016.

[22] Nabil Izzaatie Mohamad Safiai, Nur Ain Amir, Hamidon Basri, Liyana Najwa Inche Mat, Fan Kee Hoo, Abdul Hanif Khan Yusof Khan, Wei Chao Loh, Peck Kee Chia, Vasudevan Ramachandran, Hazwan Mat Din, et al. Effectiveness and tolerability of repetitive transcranial magnetic stimulation for preventive treatment of episodic migraine: a single-centre, randomised, double-blind, sham-controlled phase 2 trial (magnet-em). *Trials*, 21(1):923, 2020.

[23] Vincenzo Di Lazzaro, Michele Dileone, Fabio Pilato, Paolo Profice, Federico Ranieri, Gabriella Musumeci, Francesco Angelucci, Mario Sabatelli, and Pietro A Tonali. Repetitive transcranial magnetic stimulation for als: a preliminary controlled study. *Neuroscience letters*, 408(2):135–140, 2006.

[24] Giampietro Zanette, Antonio Forgione, Paolo Manganotti, Antonio Fiaschi, and Stefano Tamburin. The effect of repetitive transcranial magnetic stimulation on motor performance, fatigue and quality of life in amyotrophic lateral sclerosis. *Journal of the neurological sciences*, 270(1-2):18–22, 2008.

[25] Ari A Gershon, Pinhas N Dannon, and Leon Grunhaus. Transcranial magnetic stimulation in the treatment of depression. *American Journal of Psychiatry*, 160(5):835–845, 2003.

[26] Alvaro Pascual-Leone, Belen Rubio, Federico Pallardó, and Maria Dolores Catalá. Rapid-rate transcranial magnetic stimulation of left dorsolateral prefrontal cortex in drug-resistant depression. *The Lancet*, 348(9022):233–237, 1996.

[27] Marco Diana, Tommi Raij, Miriam Melis, Aapo Nummenmaa, Lorenzo Leggio, and Antonello Bonci. Rehabilitating the addicted brain with transcranial magnetic stimulation. *Nature Reviews Neuroscience*, 18(11):685–693, 2017.

[28] Ying Shen, Xinyu Cao, Tao Tan, Chunlei Shan, Yingjie Wang, Jibin Pan, Hao He, and Ti-Fei Yuan. 10-hz repetitive transcranial magnetic stimulation of the left dorsolateral prefrontal cortex reduces heroin cue craving in long-term addicts. *Biological psychiatry*, 80(3):e13–e14, 2016.

[29] Primavera A Spagnolo and David Goldman. Neuromodulation interventions for addictive disorders: challenges, promise, and roadmap for future research. *Brain*, 140(5):1183–1203, 2017.

[30] Hartwig Siebner and John Rothwell. Transcranial magnetic stimulation: new insights into representational cortical plasticity. *Experimental brain research*, 148(1):1–16, 2003.

[31] Natalie Schaworonkow, Pedro Caldana Gordon, Paolo Belardinelli, Ulf Ziemann, Til Ole Bergmann, and Christoph Zrenner. μ-rhythm extracted with personalized eeg filters correlates with corticospinal excitability in real-time phase-triggered eeg-tms. *Frontiers in neuroscience*, 12:954, 2018.

[32] Yi-Ying Lin, Rou-Shayn Chen, and Ying-Zu Huang. Impact of operator experience on transcranial magnetic stimulation. *Clinical Neurophysiology Practice*, 7:42–48, 2022.

[33] Annika A de Goede, Esther M Ter Braack, and Michel JAM van Putten. Accurate coil positioning is important for single and paired pulse tms on the subject level. *Brain topography*, 31:917–930, 2018.

[34] Hyunsoo Shin, Hyeonseok Jeong, Wooseok Ryu, Geunhu Lee, Jaeho Lee, Doyu Kim, In-Uk Song, Yong-An Chung, and Sungon Lee. Robotic transcranial magnetic stimulation in the treatment of depression: a pilot study. *Scientific Reports*, 13(1):14074, 2023.

[35] B-U Meyer, TC Britton, H Kloten, H Steinmetz, and R Benecke. Coil placement in magnetic brain stimulation related to skull and brain anatomy. *Electroencephalography and Clinical Neurophysiology/Evoked Potentials Section*, 81(1):38–46, 1991.

[36] Uwe Herwig, Carlos Schönfeldt-Lecuona, Arthur P Wunderlich, Cyrill Von Tiesenhausen, Axel Thielscher, Henrik Walter, and Manfred Spitzer. The navigation of transcranial magnetic stimulation. *Psychiatry Research: Neuroimaging*, 108(2):123–131, 2001.

[37] Adriana Bastos Conforto, Werner J Z'Graggen, Alexandra S Kohl, Kai M Rösler, and Alain Kaelin-Lang. Impact of coil position and electrophysiological monitoring on determination of motor thresholds to transcranial magnetic stimulation. *Clinical neurophysiology*, 115(4):812–819, 2004.

[38] Roland Sparing, Dorothee Buelte, Ingo G Meister, Tomás Pauš, and Gereon R Fink. Transcranial magnetic stimulation and the challenge of coil placement: a comparison of conventional and stereotaxic neuronavigational strategies. *Human brain mapping*, 29(1):82–96, 2008.

[39] Luis J Gomez, Moritz Dannhauer, and Angel V Peterchev. Fast computational optimization of tms coil placement for individualized electric field targeting. *Neuroimage*, 228:117696, 2021.

[40] Arno M Janssen, Thom F Oostendorp, and Dick F Stegeman. The coil orientation dependency of the electric field induced by tms for m1 and other brain areas. *Journal of neuroengineering and rehabilitation*, 12(1):47, 2015.

[41] Kevin A Caulfield, Holly H Fleischmann, Claire E Cox, Julia P Wolf, Mark S George, and Lisa M McTeague. Neuronavigation maximizes accuracy and precision in tms positioning: Evidence from 11,230 distance, angle, and electric field modeling measurements. *Brain stimulation*, 15(5):1192–1205, 2022.

[42] Lars Richter, Peter Trillenberg, Achim Schweikard, and Alexander Schlaefer. Stimulus intensity for hand held and robotic transcranial magnetic stimulation. *Brain stimulation*, 6(3):315–321, 2013.

[43] Nicholas Paul Holmes and Lotte Meteyard. Subjective discomfort of tms predicts reaction times differences in published studies. *Frontiers in psychology*, 9:1989, 2018.

[44] L. Richter, L. Matthäus, and A. Schlaefer, A.and Schweikard. Fast robotic compensation of spontaneous head motion during transcranial magnetic stimulation (tms). *IET Conference Proceedings*, pages 872–877, 2010.

[45] Parham M Kebria, Saeid Nahavandi, Peter Enticott, and Fernando Bello. Haptically-enabled robotic teleoperation for transcranial magnetic stimulation (teletms). In *2023 IEEE International Conference on Systems, Man, and Cybernetics (SMC)*, pages 2100–2105. IEEE, 2023.

[46] Alessia Noccaro, Alessandro Mioli, Marco D'Alonzo, Mattia Pinardi, Giovanni Di Pino, and Domenico Formica. Development and validation of a novel calibration methodology and control approach for robot-aided transcranial magnetic stimulation (tms). *IEEE Transactions on Biomedical Engineering*, 68(5):1589–1600, 2021.

[47] Zecai Lin, Xin Wang, and Jian Yang. Trajectory tracking control of robotic transcranial magnetic stimulation. *International Journal of Intelligent Computing and Cybernetics*, 12(2):245–259, 2019.

[48] WN Wan Zakaria, Razali Tomari, and Rafidah Ngadengon. Active head motion compensation of tms robotic system using neuro-fuzzy estimation. In *MATEC Web of Conferences*, volume 56, page 07001. EDP Sciences, 2016.

[49] Lucile Zorn, Pierre Renaud, Bernard Bayle, Laurent Goffin, Cyrille Lebosse, Michel de Mathelin, and Jack Foucher. Design and evaluation of a robotic system for transcranial magnetic stimulation. *IEEE Transactions on Biomedical Engineering*, 59(3):805–815, 2011.

[50] Jaewoo Kim and Gi-Hun Yang. Manipulator control of the robotized tms system with incurved tms coil case. *Applied Sciences*, 14(23):11441, 2024.

[51] Prakarn Jaroonsorn, Paramin Neranon, Pruittikorn Smithmaitrie, and Charoenyutr Dechwayukul. Robot-assisted transcranial magnetic stimulation using hybrid position/force control. *Advanced Robotics*, 34(24):1559–1570, 2020.

[52] Robert Hickson, Kayla Huynh, Linden B Aly, Jerome A Yesavage, Noah S Philip, F Andrew Kozel, and Michelle R Madore. Predictors of dropout from tms for treatment resistant depression. *Transcranial Magnetic Stimulation*, 2:100085, 2025.

[53] Sylvain Harquel, Julien Diard, Estelle Raffin, Brice Passera, Gaelle Dall'Igna, Christian Marendaz, Olivier David, and Alan Chauvin. Automatized set-up procedure for transcranial magnetic stimulation protocols. *Neuroimage*, 153:307–318, 2017.

[54] Ioannis Xygonakis, Riccardo Seganfreddo, Mazin Hamad, Samuel Schneider, Axel Schröder, Sandro M Krieg, Bernhard Meyer, Lorenzo Chiari, Melissa Zavaglia, and Sami Haddadin. Transcranial magnetic stimulation robotic assistant: towards a fully automated stimulation session. In *2024 10th IEEE RAS/EMBS International Conference for Biomedical Robotics and Biomechatronics (BioRob)*, pages 1401–1408. IEEE, 2024.

[55] Renan H Matsuda, Victor H Souza, Thais C Marchetti, Ana M Soto, Olli-Pekka Kahilakoski, Andrey Zhdanov, Victor HE Malheiro, Mikael Laine, Mikko Nyrhinen, Heikki Sinisalo, et al. Robotic–electronic platform for autonomous and accurate transcranial magnetic stimulation targeting. *Brain Stimulation: Basic, Translational, and Clinical Research in Neuromodulation*, 17(2):469–472, 2024.

[56] Michael Moche, Robert Trampel, Thomas Kahn, and Harald Busse. Navigation concepts for mr image-guided interventions. *Journal of Magnetic Resonance Imaging: An Official Journal of the International Society for Magnetic Resonance in Medicine*, 27(2):276–291, 2008.

[57] Roch Comeau. Neuronavigation for transcranial magnetic stimulation. In *Transcranial magnetic stimulation*, pages 31–56. Springer, 2014.

[58] Cyrille Lebossé, Pierre Renaud, Bernard Bayle, Michel De Mathelin, Olivier Piccin, and Jack Foucher. A robotic system for automated image-guided transcranial magnetic stimulation. In *2007 IEEE/NIH Life Science Systems and Applications Workshop*, pages 55–58. IEEE, 2007.

[59] Romuald Ginhoux, Pierre Renaud, Lucile Zorn, Laurent Goffin, Bernard Bayle, Jack Foucher, Julien Lamy, Jean-Paul Armspach, and Michel de Mathelin. A custom robot for transcranial magnetic stimulation: first assessment on healthy subjects. In *2013 35th Annual International Conference of the IEEE Engineering in Medicine and Biology Society (EMBC)*, pages 5352–5355. IEEE, 2013.

[60] Adrianna Giuffre, Cynthia K Kahl, Ephrem Zewdie, James G Wrightson, Anna Bourgeois, Elizabeth G Condliffe, and Adam Kirton. Reliability of robotic transcranial magnetic stimulation motor mapping. *Journal of Neurophysiology*, 2021.

[61] Cynthia K Kahl, Rose Swansburg, Tasmia Hai, James G Wrightson, Tiffany Bell, Jean-François Lemay, Adam Kirton, and Frank P MacMaster. Differences in neurometabolites and transcranial magnetic stimulation motor maps in children with attention-deficit/hyperactivity disorder. *Journal of Psychiatry and Neuroscience*, 47(4):E239–E249, 2022.

[62] Hyunsoo Shin, Wooseok Ryu, Sungtaek Cho, Woosung Yang, and Sungon Lee. Development of a spherical positioning robot and neuro-navigation system for precise and repetitive non-invasive brain stimulation. *Applied Sciences*, 9(21):4561, 2019.

[63] Jack L Lancaster, Shalini Narayana, Dennis Wenzel, James Luckemeyer, John Roby, and Peter Fox. Evaluation of an image-guided, robotically positioned transcranial magnetic stimulation system. *Human brain mapping*, 22(4):329–340, 2004.

[64] Lars Matthäus. A robotic assistance system for transcranial magnetic stimulation and its application to motor cortex mapping. 2008.

[65] M Finke, T Fadini, S Kantelhardt, A Giese, L Matthaus, and A Schweikard. Brain-mapping using robotized tms. In *2008 30th Annual International Conference of the IEEE Engineering in Medicine and Biology Society*, pages 3929–3932. IEEE, 2008.

[66] Lars Richter. *Robotized transcranial magnetic stimulation*. Springer, 2013.

[67] Giuseppe Pennimpede, Luca Spedaliere, Domenico Formica, Giovanni Di Pino, Loredana Zollo, Giovanni Pellegrino, Vincenzo Di Lazzaro, and Eugenio Guglielmelli. Hot spot hound: A novel robot-assisted platform for enhancing tms performance. In *2013 35th Annual International Conference of the IEEE Engineering in Medicine and Biology Society (EMBC)*, pages 6301–6304. IEEE, 2013.

[68] Stefan M Goetz, I Cassie Kozyrkov, Bruce Luber, Sarah H Lisanby, David LK Murphy, Warren M Grill, and Angel V Peterchev. Accuracy of robotic coil positioning during transcranial magnetic stimulation. *Journal of neural engineering*, 16(5):054003, 2019.

[69] Alessia Noccaro, Luigi Raiano, Giovanni Di Pino, and Domenico Formica. Evaluation of hand-eye and robot-world calibration algorithms for tms application. pages 1115–1119, 2018.

[70] Lari M Koponen, Jaakko O Nieminen, and Risto J Ilmoniemi. Multi-locus transcranial magnetic stimulation—theory and implementation. *Brain Stimulation*, 11(4):849–855, 2018.

[71] Jaakko O Nieminen, Heikki Sinisalo, Victor H Souza, Mikko Malmi, Mikhail Yuryev, Aino E Tervo, Matti Stenroos, Diego Milardovich, Juuso T Korhonen, Lari M Koponen, et al. Multi-locus transcranial magnetic stimulation system for electronically targeted brain stimulation. *Brain Stimulation*, 15(1):116–124, 2022.

[72] W.N. Wan Zakaria, Razali Tomari, and Rafidah Ngadengon. Active head motion compensation of tms robotic system using neuro-fuzzy estimation. *MATEC Web of Conferences*, 56:07001, 2016.

[73] Jan J de Jong, Arno HA Stienen, Volkert van der Wijk, Martijn Wessels, and Herman van der Kooij. A method for evaluation and comparison of parallel robots for safe human interaction, applied to robotic tms. In *2012 4th IEEE RAS & EMBS International Conference on Biomedical Robotics and Biomechatronics (BioRob)*, pages 986–991. IEEE, 2012.

[74] Jakob Nielsen. *Usability engineering*. Morgan Kaufmann, 1994.

[75] John Sweller. Cognitive load during problem solving: Effects on learning. *Cognitive science*, 12(2):257–285, 1988.

[76] Simone Rossi, Mark Hallett, Paolo M Rossini, Alvaro Pascual-Leone, Safety of TMS Consensus Group, et al. Safety, ethical considerations, and application guidelines for the use of transcranial magnetic stimulation in clinical practice and research. *Clinical neurophysiology*, 120(12):2008–2039, 2009.

[77] Masahito Kobayashi, Takamitsu Fujimaki, Ban Mihara, and Takayuki Ohira. Repetitive transcranial magnetic stimulation once a week induces sustainable long-term relief of central poststroke pain. *Neuromodulation: Technology at the Neural Interface*, 18(4):249–254, 2015.

[78] Jean-Pascal Lefaucheur, Nathalie André-Obadia, Andrea Antal, Samar S Ayache, Chris Baeken, David H Benninger, Roberto M Cantello, Massimo Cincotta, Mamede de Carvalho, Dirk De Ridder, et al. Evidence-based guidelines on the therapeutic use of repetitive transcranial magnetic stimulation (rtms). *Clinical neurophysiology*, 125(11):2150–2206, 2014.

[79] Paolo Maria Rossini, David Burke, Robert Chen, Leonardo G Cohen, Zafiris Daskalakis, R Di Iorio, Vincenzo Di Lazzaro, F Ferreri, PB Fitzgerald, Mark S George, et al. Non-invasive electrical and magnetic stimulation of the brain, spinal cord, roots and peripheral nerves: Basic principles and procedures for routine clinical and research application. an updated report from an ifcn committee. *Clinical neurophysiology*, 126(6):1071–1107, 2015.

[80] Rachel E Sondergaard, Davide Martino, Zelma HT Kiss, and Elizabeth G Condliffe. Tms motor mapping methodology and reliability: a structured review. *Frontiers in Neuroscience*, 15:709368, 2021.

[81] Cynthia K Kahl, Adam Kirton, Tamara Pringsheim, Paul E Croarkin, Ephrem Zewdie, Rose Swansburg, James Wrightson, Lisa Marie Langevin, and Frank P Macmaster. Bilateral transcranial magnetic stimulation of the supplementary motor area in children with tourette syndrome. *Developmental Medicine & Child Neurology*, 63(7):808–815, 2021.

[82] Sven Rainer Kantelhardt, Tommaso Fadini, Markus Finke, Kai Kallenberg, Jakob Siemerkus, Volker Bockermann, Lars Matthaeus, Walter Paulus, Achim Schweikard, Veit Rohde, et al. Robot-assisted image-guided transcranial magnetic stimulation for somatotopic mapping of the motor cortex: a clinical pilot study. *Acta neurochirurgica*, 152(2):333–343, 2010.

[83] Jeff G Grab, Ephrem Zewdie, Helen L Carlson, H-C Kuo, Patrick Ciechanski, Jacquie Hodge, A Giuffre, and A Kirton. Robotic tms mapping of motor cortex in the developing brain. *Journal of Neuroscience Methods*, 309:41–54, 2018.

[84] Charles Quesada, Benjamin Pommier, Camille Fauchon, Claire Bradley, Christelle Créac'h, François Vassal, and Roland Peyron. Robot-guided neuronavigated repetitive transcranial magnetic stimulation (rtms) in central neuropathic pain. *Archives of physical medicine and rehabilitation*, 99(11):2203–2215, 2018.

[85] Joseph Taylor, Jing Li, Christopher Lin, Emma Jones, Summer Frandsen, Claudia Becker, William Drew, Dania Haj-Darwish, Sandrine Jabbour, Jessica Leach, et al. Symptom-specific brain circuit stimulation: A head-to-head randomized trial. 2024.

[86] Pablo Solana, Omar Escámez, Daniel Casasanto, Ana B Chica, and Julio Santiago. No support for a causal role of primary motor cortex in construing meaning from language: An rtms study. *Neuropsychologia*, 196:108832, 2024.

[87] Mar Martín-Signes, Cristina Cano-Melle, and Ana B Chica. Fronto-parietal networks underlie the interaction between executive control and conscious perception: Evidence from tms and dwi. *Cortex*, 134:1–15, 2021.

[88] Alina Davydova, Julia Sheronova, Vladimir Kosonogov, Vasily Klucharev, and Anna Shestakova. Tms study of the role of the medial and dorsolateral prefrontal cortex in the post-decisional spreading of alternatives. In *2022 Fourth International Conference Neurotechnologies and Neurointerfaces (CNN)*, pages 17–20. IEEE, 2022.

[89] Steven L Wolf, Andrew J Butler, Georgette I Campana, Trinity A Parris, Danielle M Struys, Sarah R Weinstein, and Paul Weiss. Intra-subject reliability of parameters contributing to maps generated by transcranial magnetic stimulation in able-bodied adults. *Clinical neurophysiology*, 115(8):1740–1747, 2004.

[90] Andrew E Littmann, Colleen L McHenry, and Richard K Shields. Variability of motor cortical excitability using a novel mapping procedure. *Journal of neuroscience methods*, 214(2):137–143, 2013.

[91] J Rodseth, EP Washabaugh, and C Krishnan. A novel low-cost approach for navigated transcranial magnetic stimulation. *Restorative neurology and neuroscience*, 35(6):601–609, 2017.

[92] Neville Hogan. Impedance control: An approach to manipulation: Part i—theory. 1985.

[93] Oussama Khatib. A unified approach for motion and force control of robot manipulators: The operational space formulation. *IEEE Journal on Robotics and Automation*, 3(1):43–53, 1987.

[94] Valerio Ortenzi, Rustam Stolkin, J Kuo, and M Mistry. Hybrid motion/force control: a review. *Advanced Robotics*, 31(19-20):1102–1113, 2017.

[95] E. Hirasaki, S. T. Moore, T. Raphan, and B. Cohen. Effects of walking velocity on vertical head and body movements during locomotion. *Experimental brain research*, 127(2):117–130, 1999.

[96] Keith Ord. Outliers in statistical data: V. barnett and t. lewis, 1994, 3rd edition, (john wiley & sons, chichester), 584 pp., £55.00, isbn 0-471-93094-6. *International Journal of Forecasting*, 12(1):175–176, 1996. Probability Judgmental Forecasting.

[97] Alexa Riehle and Eilon Vaadia. *Motor cortex in voluntary movements: a distributed system for distributed functions*. CRC Press, 2004.

[98] Carolien M Toxopeus, Bauke M de Jong, Gopal Valsan, Bernard A Conway, Klaus L Leenders, and Natasha M Maurits. Direction of movement is encoded in the human primary motor cortex. *PLoS One*, 6(11):e27838, 2011.

[99] Christopher D Cowper-Smith, Esther YY Lau, Carl A Helmick, Gail A Eskes, and David A Westwood. Neural coding of movement direction in the healthy human brain. *PloS one*, 5(10):e13330, 2010.

[100] Michal Eisenberg, Lior Shmuelof, Eilon Vaadia, and Ehud Zohary. Functional organization of human motor cortex: directional selectivity for movement. *Journal of Neuroscience*, 30(26):8897–8905, 2010.

[101] Juha Silvanto and Zaira Cattaneo. Nonlinear interaction between stimulation intensity and initial brain state: evidence for the facilitatory/suppressive range model of online tms effects. *Neuroscience letters*, 742:135538, 2021.

[102] Emilio Chiappini, Sonia Turrini, Francesca Fiori, Mariagrazia Benassi, Alessia Tessari, Giuseppe di Pellegrino, and Alessio Avenanti. You are as old as the connectivity you keep: Distinct neurophysiological mechanisms underlying age-related changes in hand dexterity and strength. *Archives of Medical Research*, 56(1):103031, 2025.

[103] Sivakumar Balasubramanian, Alejandro Melendez-Calderon, and Etienne Burdet. A robust and sensitive metric for quantifying movement smoothness. *IEEE transactions on biomedical engineering*, 59(8):2126–2136, 2011.

[104] Juha Silvanto, Neil Muggleton, and Vincent Walsh. State-dependency in brain stimulation studies of perception and cognition. *Trends in cognitive sciences*, 12(12):447–454, 2008.

[105] Martin Sommer, Joseph Classen, Leonardo G Cohen, and Mark Hallett. Time course of determination of movement direction in the reaction time task in humans. *Journal of Neurophysiology*, 86(3):1195–1201, 2001.

[106] Hartwig R Siebner, Nicolas Lang, Vincenzo Rizzo, Michael A Nitsche, Walter Paulus, Roger N Lemon, and John C Rothwell. Preconditioning of low-frequency repetitive transcranial magnetic stimulation with transcranial direct current stimulation: evidence for homeostatic plasticity in the human motor cortex. *Journal of Neuroscience*, 24(13):3379–3385, 2004.

[107] Mads Gylling Safeldt, Leo Tomasevic, Anke Karabanov, H Siebner, and Kristoffer H Madsen. Towards brain-state dependent transcranial magnetic stimulation: Targeting the phase of oscillatory neocortical activity with singe-pulse tms. *Brain Stimulation: Basic, Translational, and Clinical Research in Neuromodulation*, 10(2):449–450, 2017.

[108] Debora Desideri, Christoph Zrenner, Ulf Ziemann, and Paolo Belardinelli. Phase of sensorimotor μ-oscillation modulates cortical responses to transcranial magnetic stimulation of the human motor cortex. *The Journal of physiology*, 597(23):5671–5686, 2019.

[109] Claudia Bigoni, Sara Pagnamenta, Andéol Cadic-Melchior, Michele Bevilacqua, Sylvain Harquel, Estelle Raffin, and Friedhelm C Hummel. Mep and tep features variability: is it just the brain-state? *Journal of Neural Engineering*, 21(1):016011, 2024.

[110] L Leon Chen, Radhika Madhavan, Benjamin I Rapoport, and William S Anderson. Real-time brain oscillation detection and phase-locked stimulation using autoregressive spectral estimation and time-series forward prediction. *IEEE transactions on Biomedical Engineering*, 60(3):753–762, 2011.

[111] Christoph Zrenner, Debora Desideri, Paolo Belardinelli, and Ulf Ziemann. Real-time eeg-defined excitability states determine efficacy of tms-induced plasticity in human motor cortex. *Brain stimulation*, 11(2):374–389, 2018.

[112] Sina Shirinpour, Ivan Alekseichuk, Kathleen Mantell, and Alexander Opitz. Experimental evaluation of methods for real-time eeg phase-specific transcranial magnetic stimulation. *Journal of neural engineering*, 17(4):046002, 2020.

[113] Miles Wischnewski, Zachary J Haigh, Sina Shirinpour, Ivan Alekseichuk, and Alexander Opitz. The phase of sensorimotor mu and beta oscillations has the opposite effect on corticospinal excitability. *Brain stimulation*, 15(5):1093–1100, 2022.

[114] Leo Tomasevic and Hartwig Roman Siebner. Peak-projection algorithm to target the phase of cortical oscillations in real-time. In *2018 EMF-Med 1st World Conference on Biomedical Applications of Electromagnetic Fields (EMF-Med)*, pages 1–2. IEEE, 2018.

[115] Farrokh Mansouri, Katharine Dunlop, Peter Giacobbe, Jonathan Downar, and José Zariffa. A fast eeg forecasting algorithm for phase-locked transcranial electrical stimulation of the human brain. *Frontiers in neuroscience*, 11:401, 2017.

[116] Kristoffer Hougaard Madsen, Anke Ninija Karabanov, Lærke Gebser Krohne, Mads Gylling Safeldt, Leo Tomasevic, and Hartwig Roman Siebner. No trace of phase: Corticomotor excitability is not tuned by phase of pericentral mu-rhythm. *Brain stimulation*, 12(5):1261–1270, 2019.

[117] John R Knott. Regarding the american electroencephalographic society guidelines for standard electrode position nomenclature: a commentary on the proposal to change the 10-20 electrode designators. *Journal of Clinical Neurophysiology*, 10(1):123–124, 1993.

[118] Natalie Schaworonkow, Jochen Triesch, Ulf Ziemann, and Christoph Zrenner. Eeg-triggered tms reveals stronger brain state-dependent modulation of motor evoked potentials at weaker stimulation intensities. *Brain stimulation*, 12(1):110–118, 2019.

[119] Paolo M Rossini and Simone Rossi. Transcranial magnetic stimulation: diagnostic, therapeutic, and research potential. *Neurology*, 68(7):484–488, 2007.

[120] Christoph Zrenner, Paolo Belardinelli, Florian Müller-Dahlhaus, and Ulf Ziemann. Closed-loop neuroscience and non-invasive brain stimulation: a tale of two loops. *Frontiers in cellular neuroscience*, 10:92, 2016.

[121] Mark G Stokes, Christopher D Chambers, Ian C Gould, Tracy R Henderson, Natasha E Janko, Nicholas B Allen, and Jason B Mattingley. Simple metric for scaling motor threshold based on scalp-cortex distance: application to studies using transcranial magnetic stimulation. *Journal of neurophysiology*, 94(6):4520–4527, 2005.

[122] Daniel T Corp, Hannah GK Bereznicki, Gillian M Clark, George J Youssef, Peter J Fried, Ali Jannati, Charlotte B Davies, Joyce Gomes-Osman, Julie Stamm, Sung Wook Chung, et al. Large-scale analysis of interindividual variability in theta-burst stimulation data: Results from the 'big tms data collaboration'. *Brain stimulation*, 13(5):1476–1488, 2020.

[123] Paula Davila-Pérez, Ali Jannati, Peter J Fried, Javier Cudeiro Mazaira, and Alvaro Pascual-Leone. The effects of waveform and current direction on the efficacy and test–retest reliability of transcranial magnetic stimulation. *Neuroscience*, 393:97–109, 2018.

[124] Wenzhi Bai, Andrew Weightman, Rory J O'Connor, Zhengtao Ding, Mingming Zhang, Sheng Quan Xie, and Zhenhong Li. Robot-assisted transcranial magnetic stimulation (robo-tms): A review. *IEEE Transactions on Neural Systems and Rehabilitation Engineering*, 2025.